SPACE WEATHER, VOL. 5, S09003, doi:10.1029/2006SW000260, 2007

GPS and ionospheric scintillations

P. M. Kintner,[1] B. M. Ledvina,[2] and E. R. de Paula[3]

Received 15 June 2006; revised 12 April 2007; accepted 21 April 2007; published 7 September 2007.

[1] Ionospheric scintillations are one of the earliest known effects of space weather. Caused by ionization density irregularities, scintillating signals change phase unexpectedly and vary rapidly in amplitude. GPS signals are vulnerable to ionospheric irregularities and scintillate with amplitude variations exceeding 20 dB. GPS is a weak signal system and scintillations can interrupt or degrade GPS receiver operation. For individual signals, interruption is caused by fading of the in-phase and quadrature signals, making the determination of phase by a tracking loop impossible. Degradation occurs when phase scintillations introduce ranging errors or when loss of tracking and failure to acquire signals increases the dilution of precision. GPS scintillations occur most often near the magnetic equator during solar maximum, but they can occur anywhere on Earth during any phase of the solar cycle. In this article we review the subject of GPS and ionospheric scintillations for scientists interested in space weather and engineers interested in the impact of scintillations on GPS receiver design and use.

Citation: Kintner, P. M., B. M. Ledvina, and E. R. de Paula (2007), GPS and ionospheric scintillations, *Space Weather*, *5*, S09003, doi:10.1029/2006SW000260.

1. Introduction

[2] One of the first known effects of space weather was fluctuations in the amplitude and phase of radio signals that transit the ionosphere [*Hey et al.*, 1946]. The fluctuations are called scintillations which, if sufficiently intense, degrade the signal quality, reduce its information content, or cause failure of the signal reception. In this paper we will focus on the effect of scintillations on Global Positioning System (GPS) signals and receivers. Sufficiently intense signal fluctuations cause GPS receivers to stop tracking the signals from GPS satellites in a process sometimes called "loss of lock." This may increase navigation errors or, in some cases, cause navigation failure. Acquiring or reacquiring satellite signals becomes problematic during scintillations. Alternately, the fluctuations may be used to investigate the behavior of the ionosphere. Understanding the effect of scintillations on GPS receivers and creating strategies to mitigate those effects requires an understanding of ionospheric science and GPS receiver engineering. New and planned Global Navigation Satellite System (GNSS) signals, satellites, and systems such as modernized GPS, Galileo, and Space-Based Augmentation Systems (SBAS) may mitigate some aspects of scintillations but will also introduce new vulnerabilities. With the goal of benefiting both space scientists and GPS system engineers, this paper is an overview of scintillations, GPS receivers, and the effects of GPS scintillations on GPS receivers.

[3] The expression "scintillations" typically refers to rapid amplitude and phase fluctuations in a received electromagnetic wave. The cause may be diffractive when electromagnetic waves are scattered in an irregular medium composed of many small changes in the index of refraction. An impinging plane wave enters such a medium with a spatially uniform phase and exits the medium with a spatially irregular phase. After propagation to a receiver, the irregular phases may combine either constructively or destructively to increase or decrease the wave amplitude. Alternately, the cause may be refractive when an electromagnetic wave enters a medium of either increased or decreased phase velocity. A plane wave remains a plane wave but the phase observed by a receiver will change as the integrated phase shift across the medium changes. Scintillations have been observed in natural and man-made signals for many decades [see, e.g., *Briggs and Parkin*, 1963; *Kent*, 1959].

[4] Ionospheric scintillations are caused when electromagnetic signals propagate through an irregular ionosphere. Any electromagnetic signal with frequencies above the X-mode or O-mode cutoffs, typically one to a few tens of MHz and located near the plasma frequency, can propagate through the ionosphere. GPS satellite signal frequencies are chosen to be well above these cutoffs so that the signals propagate through the ionosphere with

[1]School of Electrical and Computer Engineering, Cornell University, Ithaca, New York, USA.
[2]Applied Research Laboratories, University of Texas at Austin, Austin, Texas, USA.
[3]Instituto Nacional de Pesquisas Espaciais, DAE, São Josédos Campos, São Paulo, Brazil.

little change when the ionosphere is uniform. However, when the ionosphere is irregular, diffractive scintillations will occur. The degree to which the ionospheric irregularities produce scintillations is determined by the frequency of the signal compared to the plasma frequency and the strength of the irregularities. Denser plasmas can produce scintillations at higher frequencies and more irregular plasmas produce stronger amplitude scintillations. The temporal behavior of diffractive scintillations depends on the Fresnel length of the scintillations (see section 2.2), the drift speed of the ionosphere, and the relative velocities of the satellites and receivers [*Kintner et al.*, 2004].

[5] Initial studies of ionospheric scintillations were primarily in the VHF and UHF radio bands and focused on the effect of the scintillations on communication signals [*Whitney and Basu*, 1977]. Early investigators demonstrated that the most likely regions for observing scintillations were near the magnetic equator, including the Appleton anomalies, and within the auroral oval and polar cap [*Basu et al.*, 1988]; that the scintillation amplitudes demonstrated a solar cycle dependence with maximum amplitudes at the solar cycle maximum when solar UV fluxes and ionospheric density were also a maximum [*Briggs*, 1964]; and that equatorial scintillations demonstrated a seasonal dependence, depending on the longitude [*Aarons et al.*, 1980b; *Tsunoda*, 1985].

[6] With the introduction of L-band communication links on satellites, scintillations were investigated at higher frequencies, including those used by the GPS satellites [*Basu et al.*, 1980; *Aarons and Basu*, 1994]. Since those early investigations, the use of GPS in civilian applications has added exponentially to DOD applications of GPS, and the importance of space weather, specifically scintillations, is a cause of growing concern, particularly to those new applications that are life-critical such as GPS-aided aviation [*Conker et al.*, 2003; *Dehel et al.*, 2004]. In this case scintillations are as much an engineering concern as they are a science concern. While scintillations can be used to investigate the irregularities or propagation medium that produce them, the societal impact depends on the scintillation morphology and detailed characteristics as well as the GPS architecture, signals and receiver designs.

[7] The space segment of the GPS architecture is a constellation of 24–28 satellites in circular orbits at 26,600 km radius with a 55 degree inclination. They are in six orbital planes whose ascending nodes are equally spaced 60 degrees apart. Each satellite transmits at exactly the same two frequencies: L1 = 1575.42 MHz and L2 = 1227.6 MHz. The satellite signals are separated by modulating each carrier with a pseudorandom noise (PRN) code unique to each satellite, forming a code division multiple access link (CDMA). There are two codes on L1: the coarse acquisition code (C/A) and the encrypted precise code (P(Y)). On L2 only the P(Y) code is transmitted. Most civilian receivers only use the L1 C/A code signal. This is adequate for accuracies of 5–15 m. Military receivers use the P(Y) code on L1 and L2, achieving accuracies of 3–5 m. By receiving on two frequencies, the dispersive properties of the refractive ionosphere can be measured, the ionospheric total electron content (TEC) calculated, and the ionospheric error removed. Some civilian receivers can also calculate TEC using L1 and L2 by cross-correlating the two signals against each other without knowing the encrypting bits on the P(Y) code. These receivers are typically expensive, operate in a low signal-to-noise environment, and must be stationary to avoid stressed tracking loops. These dual-frequency civilian receivers have a great variety of applications. For example, networks of them are used to create ionospheric images and to feed assimilative ionospheric models [*Saito et al.*, 1998; *Hajj et al.*, 2004; *Coster et al.*, 2005].

[8] In the next decade several new GNSS satellite systems and signals will be introduced. The first system is augmentation signals that are transmitted on the L1 frequency and contain ionospheric and ephemeris corrections derived from ground-based, dual frequency, civilian reference receivers. This includes the North American Wide Area Augmentation System (WAAS), which was commissioned on 10 July 2003; the European Geodetic Navigation Overlay System (EGNOS), which is currently being commissioned; the Japanese Multifunctional Satellite-based Augmentation System (MSAS), which is also currently being commissioned; and planned Indian GPS and Geo-Augmented Navigation (GAGAN). All of these augmentation systems share the L1 frequency using a PRN code compatible with GPS PRN codes and are transmitted from a geostationary satellite. These systems are so new that only a few investigations of scintillating signals have been reported [*Doherty et al.*, 2004; *Cerruti et al.*, 2005; *Ledvina and Makela*, 2005]. The principal difference between GPS and Space-Based Augmentation Systems (SBAS) is that the GPS ionospheric signal puncture points move whereas SBAS puncture points are stationary. Accompanying SBAS systems are the Russian GLONASS system, which currently has 12 satellites in GPS-like orbits, the European Galileo system, which recently launched its first test bed satellite accompanied by some controversy over access to the signals [*Psiaki et al.*, 2006], the planned Japanese Quasi-Zenith Satellite System (QZSS) to provide coverage in urban canyons, and the Chinese Compass system, which is currently under formulation. Finally, GPS itself is being modernized with a new civilian code on L2, allowing civilian receivers to make dual-frequency ionospheric corrections, and a new frequency and code on L5 (1176.45 MHz) in an aviation-protected band for safety-of-life operations. These new codes and frequencies should be operational between 2012 and 2015, after the next solar maximum.

[9] The remainder of this paper will focus on GPS and scintillations by discussing the theory of scintillation and irregularities, examining GPS receiver operation, and presenting GPS scintillation observations at low, middle, and high latitudes. At low latitudes the ionospheric dynamic

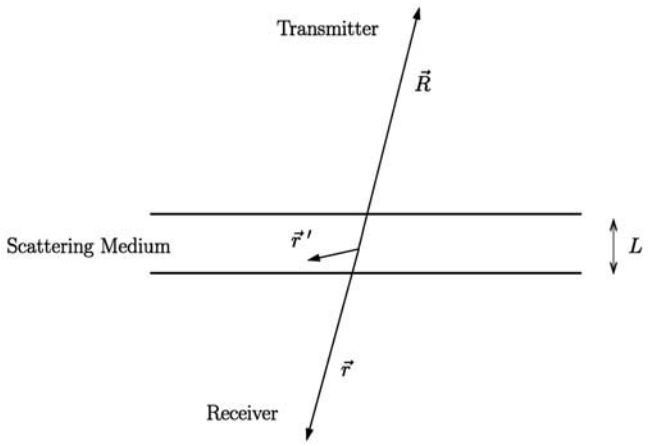

Figure 1. Coordinate system showing wave propagation through an irregularity layer.

behavior is dominated by solar tides and horizontal geomagnetic field lines. At high latitudes the ionospheric dynamic behavior is dominated by the solar wind and electron precipitation (aurora borealis and aurora australis). At midlatitudes, ionospheric dynamics are dominated by the inner magnetosphere and neutral winds, of which our knowledge is incomplete. We conclude with an examination of future navigation signals and systems.

2. Review of Scintillation Theory

[10] Several excellent sources provide thorough information regarding scintillation theory, including *Lovelace* [1970], *Tatarskii* [1971], and *Yeh and Liu* [1982]. The extent of this review outlines the one-dimensional weak scattering case, which involves single, forward scattering of radio waves by ionospheric electron density irregularities that have wavelengths much greater than the incident radio wave's wavelength. The variations in permittivity along the ray path are assumed to be small.

2.1. Wave Propagation in a Random Media

[11] The starting point for the development of equations that describe radio wave propagation through a random scattering medium is Maxwell's equations. The result is typically the derivation of the scalar Helmholtz equation, which represents wave propagation in an irregular medium where single, forward scattering is predominant and where the irregularities have scale sizes larger than the wavelength of the radio wave. The scalar Helmholtz wave equation is

$$\nabla^2 A + k^2[1 + \epsilon_1(\vec{r}')]A = 0 \qquad (1)$$

where A is the complex amplitude of the electric field, ε_1 is the deviation from free-space permittivity, k is the wave number of the signal, and $\vec{r}'$ describes the location of the irregularities. Solutions to this equation, typically involving a Green's function, describe the wave's propagation at a snapshot in time. This assumes that the irregularities evolve on timescales that are much slower than the wave's propagation speed through the medium.

[12] One solution, which assumes that the fluctuations in permittivity are small, that the incident signal is a plane wave, and that the irregularities' scale sizes are much larger than the Fresnel radius is [*Beach, 1998*, equation [4.26]]:

$$A(r) = -\frac{\exp[ik(r+R)]}{4\pi(r+R)}\left[1 + \frac{ik}{2}\int_{-L/2}^{L/2} \epsilon_1(0,0,z')dz'\right] \qquad (2)$$

where R is the distance from the radio wave source to the irregularities, r is the distance from the irregularities to the receiver, k is the wave number of the radio signal, the z' direction is along the ray path, and L is the thickness of the irregularity layer. Figure 1 illustrates these different measures.

[13] This result illustrates, under certain restrictive conditions, how irregularities that are primarily along the ray path affect a received radio signal. The assumption that the permittivity fluctuations primarily lie along the ray path provides the motivation for what is known as the phase screen approximation, which is discussed below.

[14] One important note is that solutions to equation (1) are a function of the wave number, which is inversely proportional to the wave frequency. This means that ionospheric scintillations of two signals at two different frequencies that are broadcast from the same satellite will be affected differently by the irregularities. The magnitude of this difference depends on the strength of the scattering.

2.2. Phase Screen Approximation

[15] As mentioned above, under certain approximations it is possible to model the primary effect on wave propagation through Fresnel-scale electron density irregularities as a function of the integral of the permittivity fluctuations along the ray path. This suggests compressing the fluctuations into a thin layer, which is known as a phase screen.

[16] The earliest work on phase screens was presented by *Booker et al.* [1950] and *Hewish* [1951]. Subsequent work can be found in the work of *Lovelace* [1970], *Buckley* [1975], and *Pidwerbetsky and Lovelace* [1989]. The phase screen model defines an infinitely thin layer that only induces phase perturbations on the incident radio wave. After passing through the screen, the induced phase perturbations evolve as the wave propagates, producing amplitude and phase scintillations. This is a simple model. It is a useful pedagogical tool and has some utility in computing statistical parameters of the irregularity layer.

[17] The spectrum of the radio wave intensity by amplitude is $I = A^*A$ [*Yeh and Liu*, 1982]:

$$\Phi_I(q) = \Phi_\phi(q)\sin^2\left(\frac{q^2 r_F^2}{8\pi}\right) \tag{3}$$

where q is the horizontal wave number of the phase fluctuations across the screen, Φ_ϕ is the power spectrum of the wave phase exciting the screen and for small changes in phase is linearly related to the irregularity density spectrum, Φ_I is the Fourier transform of the intensity autocorrelation function, and $r_F = \sqrt{2\lambda r}$ is the Fresnel radius, where λ is the incident signal's wavelength.

[18] The term $\sin^2(q^2 r_F^2/8\pi)$ in this equation is known as the Fresnel filtering function. To the first order, this function provides an upper limit on the scale size of irregularities. The upper limit of the scale size, or the Fresnel radius r_F, occurs where the $\sin^2$ term goes to one, or when the argument is equal to $(2n-1)\pi/2$ radians. The Fresnel radius at $n = 1$ is ~365 m for GPS L1 signals, assuming an irregularity layer mean altitude of 350 km and a signal path elevation of 90°.

[19] The spectrum of the phase deviations is [*Yeh and Liu*, 1982]:

$$\Phi_p(q) = \Phi_\phi(q)\cos^2\left(\frac{q^2 r_F^2}{8\pi}\right). \tag{4}$$

[20] Unlike the amplitude scintillations, the phase scintillations have a maximum at $q = 0$. The next local maximum is when the argument becomes $n\pi$ radians. For $n = 1$ this corresponds to $r_F/\sqrt{2}$ and when the amplitude spectrum (equation (3)) also goes to zero. Because the one-dimensional phase spectrum at the phase screen typically has the form $\Phi_\phi(q) \sim q^{-n}$ where n is of order 2, the majority of the phase fluctuation power is found at small q.

[21] The above model has some application in considering one-dimensional weak scattering. For strong scattering, both amplitude and phase of the incident plane wave are altered in crossing the phase screen. Also the phase screen may only be approximated as one-dimensional in specific conditions such as near the geomagnetic equator for signals from high-elevation satellites. Consideration of these more complex environments can be found in the work of *Rino and Fremouw* [1977] and *Rino* [1979a, 1979b].

2.3. Amplitude Scintillations

[22] The strength of amplitude scintillations is typically quantified by a metric called the S_4 index. The S_4 index is the ratio of the standard deviation of the signal power to the mean signal power computed over a period of time, which is

$$S_4 = \sqrt{\frac{\langle I^2\rangle - \langle I\rangle^2}{\langle I\rangle^2}} \tag{5}$$

where $I = A^*A$, and the brackets indicate ensemble averaging, which can be approximated by the time averages of I. This time period is nominally 60 s but could be arbitrarily larger or smaller, keeping in mind that the time period must be long compared to the Fresnel length divided by the irregularity drift speed.

2.4. Phase Scintillations

[23] Phase scintillations are typically produced by ionospheric irregularities at small wave numbers and near the first Fresnel radius ($r_F/\sqrt{2}$). The former quantity (small wave numbers) can be thought of as being refractive and produced by fluctuations in the integrated ionospheric plasma density along the signal path. The latter quantity (near the first Fresnel radius) is the result of interference between different phases exiting the thin screen and can be thought of as diffractive. Hence the latter quantity specifies phase deviations ordered by the Fresnel radius. The literature tends to refer to both sources as phase scintillations, although only the latter is produced by irregularities near the Fresnel radius.

[24] The refractive component of the GPS signal phase deviation produced during transit of the ionosphere is given by

$$\phi = \frac{q^2}{2c\varepsilon_0 m_e f(2\pi)^2}\int n_e d\rho \tag{6}$$

where $\int n_e d\rho$ is called the total electron content (TEC), q is the charge of an electron, m_e is the mass of an electron, ε_0 is the permittivity of free space, c is the speed of light, and f is in Hertz. In MKS units this reduces to

$$\phi = \frac{40.3}{cf}\mathrm{TEC} \tag{7}$$

[25] If the ionospheric total electron content varies so that δ TEC = 10 TECU (1 TECU = 10^{16} e/m^2) and f = 1.57542 GHz, then $\delta\phi$ = 8.58 cycles.

[26] The index for tabulating phase variation measurements is called the sigma-phi (σ_ϕ) index and is defined as the standard deviation of ϕ in radians. *Forte and Radicella* [2002] point out that the σ_ϕ index is sensitive to how data are detrended, which may admit receiver clock noise or GPS satellite motion. *Forte* [2005] and *Beach* [2006] demonstrate that failure to adequately consider irregularity dynamics may lead to false conclusions. Given the various effects of phase fluctuations as GPS receiver tracking (see section 3.3 and 6) and the significance of ionospheric gradients on WAAS integrity [*Klobuchar et al.*, 1995], a better or multiple definitions of $\sigma\phi$ are called for, both to separate the refractive and diffractive components and to be relevant for the user community.

3. GPS Receiver Signal Tracking During Ionospheric Scintillations

[27] To better understand the effects of ionospheric scintillations on a GPS receiver, it is instructive to delve into the receiver signal correlation and tracking. The

Table 1. Nominal Received GPS Signal Power and Received C/N_0

SV Block IIR-M/IIF	Frequency	P or P(Y)	C/A or L2C
Signal Power	L1	−161.5 dbW	−158.5 dBW
	L2	−161.5 dBW	−160.0 dBW
C/N_0	L1	43.5 dB-Hz	46.5 dB-Hz
	L2	43.5 dB-Hz	45 dB-Hz

correlation and tracking described here covers the GPS L1 C/A code. Nevertheless, the concepts are generally applicable to correlation and tracking of other GNSS signals.

3.1. Nominal GPS Signal Strength and Dynamic Range

[28] To appreciate the effects of scintillations on GPS signals, it is important to illustrate the nominal received GPS signal strength. GPS technical specifications for the interface between the space segment and the user segment can be found in the NAVSTAR Global Positioning System Interface Specification (7 March 2006).

[29] Table 1 shows the expected carrier-to-noise (C/N_0) ratio for a receiver tracking a satellite at zenith given a typical noise power density of -205 dBW-Hz [*Spilker*, 1996]. This estimate of the noise power density is for a receiver with an antenna, a band-pass filter, a low-noise amplifier, and a transmission line. These assumptions are reasonable, even for receivers with multiple band-pass filters and amplifiers, given that the receiver noise figure is heavily weighted by the first component after the antenna, the low noise preamplifier. The actual received C/N_0 can be 6 dB higher because the satellites are typically designed with more power than is illustrated in Table 1 because of the expected degradation in power over the satellite's lifetime. The values of C/N_0 listed in Table 1 should be compared against the values required to acquire and track GPS signals. The thresholds are dependent on receiver design but typically 33 dB-Hz is required for acquisition and 26−30 dB-Hz is required to maintain tracking lock.

[30] To understand the variations in signal power caused by scintillations, it is illustrative to compare a nonscintillating signal to one that is scintillating, as is done in Figure 2. The signal on PRN 7 is an example of a strongly scintillating signal with an S_4 index of 0.9. The signal amplitude both increases and decreases as the diffracted signals add constructively and destructively. Tracking of PRN 7 was performed using a nonreal time digital storage receiver with a Kalman filter tracking loop [*Humphreys et al.*, 2005] and most, if not all, GPS receivers would fail in this environment. The ∼1−2 dB peak-to-peak variation in the signal power of the nonscintillating signal on PRN 8 is due to signal sampling and quantization effects, finite filter bandwidth, thermal noise, interchannel modulation, receiver clock noise, and multipath.

[31] Multipath signal interference can be misconstrued as scintillations. The simplest way to determine if amplitude or phase fluctuations are due to multipath is to look at day-to-day repeatability of the fluctuations. Multipath tends to repeat from day to day because it is a function of relative satellite-receiver positioning, which nominally repeats every 24 sidereal hours.

3.2. Review of the GPS Signal Structure

[32] To understand the methods used to track GPS signals is it important to review the GPS signal structure. For simplicity, the L1 C/A code signal is described in this section. The P-code signal, which is encrypted into the P(Y) code or Y code signal, is not presented here because it requires a military-grade receiver with the encryption module and key to evaluate tracking performance and there are no published reports of P(Y) signals observed during strong ionospheric scintillations. This point is elaborated later in this section.

[33] The down-converted L1 C/A code signal has the following form in the discrete time domain:

$$y(t_i) = \sum_j A_j D_{jk} C_j \left[0.001\left(\frac{t_i - t_{jk}}{t_{jk+1} - t_{jk}}\right)\right] \cdot \cos\left\{\omega_{IF} t_i - \left[\phi_j(t_i) + \omega_{Doppj}(t_i)\right]\right\} + n_j \quad (8)$$

where t_i is the sample time, A_j is the amplitude, D_{jk} is the navigation data bit, $C_j[t]$ is the C/A code, τ_{jk} and τ_{jk+1} are the start times of the received k^{th} and k + 1st C/A code periods, ω_{IF} is the intermediate frequency corresponding to the L1 carrier frequency, $\omega_{Doppj}(t_i)$ is the carrier Doppler shift frequency, $\phi_j(t_i)$ is the carrier phase perturbation due to accumulated delta range, n_j is the receiver noise, and the subscript j refers to a particular GPS satellite. The summation is over all visible GPS satellites. The negative sign in front of $\phi(t_i) + \omega_{Doppj}(t_i)$ assumes that the RF front end uses high-side mixing. The C/A code has a length of 1023 chips and a chipping rate of 1.023 MHz.

[34] A GPS receiver works with correlations between the received signal carrier and PRN code and a replica of the carrier and signal PRN code produced in the receiver. The correlations between the received signal and replica are used to acquire and track the signal. The replica is constructed from the carrier replica and the C/A code

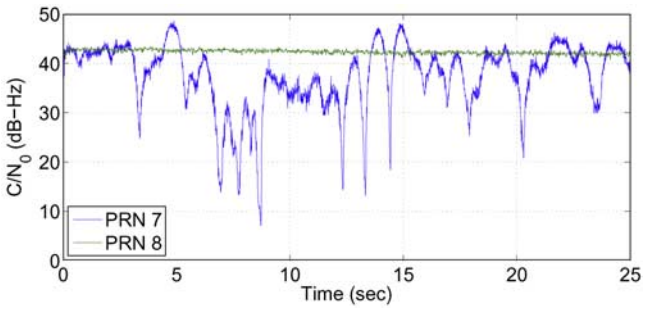

Figure 2. Comparison of scintillating and nonscintillating GPS signals.

replica (C_j). Two carrier replica signals are used: an in-phase signal and a quadrature signal. When mixed with the code replica (C_j), they form the in-phase and quadrature replicas used to acquire and track the GPS signals:

$$y_{Ij}(t_i) = C_j\left[0.001\left(\frac{t_i - \hat{\tau}_{jk}}{\hat{\tau}_{jk+1} - \hat{\tau}_{jk}}\right)\right] \cdot \cos\left\{\omega_{IF}t_i - \left[\hat{\phi}_{jk} + \hat{\omega}_{Doppjk}\left(t_i - \hat{\tau}_{jk}\right)\right]\right\} \quad (9)$$

$$y_{Qj}(t_i) = -C_j\left[0.001\left(\frac{t_i - \hat{\tau}_{jk}}{\hat{\tau}_{jk+1} - \hat{\tau}_{jk}}\right)\right] \cdot \sin\left\{\omega_{IF}t_i - \left[\hat{\phi}_{jk} + \hat{\omega}_{Doppjk}\left(t_i - \hat{\tau}_{jk}\right)\right]\right\} \quad (10)$$

where equations (9) and (10) apply during the k^{th} C/A code period. In these equations, $\hat{\tau}_{jk}$ and $\hat{\tau}_{jk+1}$ are the receiver's estimates of the start times of the k^{th} and k + 1st code periods, $\hat{\phi}_{jk}$ is the estimated carrier phase at time $\hat{\tau}_{jk}$, and $\hat{\omega}_{Doppjk}$ is the estimated carrier Doppler shift during the k^{th} code period. Note that the data bits D_{jk}, amplitude A_j, and noise are not estimated but are measured as part of the correlation process.

[35] A typical receiver computes the estimates $\hat{\tau}_{jk}$, $\hat{\tau}_{jk+1}$, $\hat{\phi}_{jk}$, and $\hat{\omega}_{Doppjk}$ by various means described by *Van Dierendonck* [1996]. These include open-loop acquisition methods and closed-loop signal tracking methods such as a delay-lock loop to compute $\hat{\tau}_{jk}$ and $\hat{\tau}_{jk+1}$ and a phase-lock loop or a frequency-lock loop to compute $\hat{\phi}_{jk}$ and $\hat{\omega}_{Doppjk}$.

[36] The receiver correlates the carrier and code replicas ((9) and (10)) with the incoming signal (8) to compute the following in-phase and quadrature accumulations:

$$I_{jk}(\Delta) = \sum_{i=i_k}^{i_k+N_k} y(t_i)C_j\left[0.001\left(\frac{t_i + \Delta - \hat{\tau}_{jk}}{\hat{\tau}_{jk+1} - \hat{\tau}_{jk}}\right)\right] \cdot \cos\left\{\omega_{IF}t_i - \left[\hat{\phi}_{jk} + \hat{\omega}_{Doppjk}\left(t_i - \hat{\tau}_{jk}\right)\right]\right\} \quad (11)$$

$$Q_{jk}(\Delta) = -\sum_{i=i_k}^{i_k+N_k} y(t_i)C_j\left[0.001\left(\frac{t_i + \Delta - \hat{\tau}_{jk}}{\hat{\tau}_{jk+1} - \hat{\tau}_{jk}}\right)\right] \cdot \sin\left\{\omega_{IF}t_i - \left[\hat{\phi}_{jk} + \hat{\omega}_{Doppjk}\left(t_i - \hat{\tau}_{jk}\right)\right]\right\} \quad (12)$$

where i_k is the index of the first RF front end sample time that obeys $\hat{\tau}_{jk} \le t_{ik}$ and N_k + 1 is the total number of samples that obey $\hat{\tau}_{jk} \le t_i < \hat{\tau}_{jk+1}$. The time offset Δ is introduced in the receiver that causes the replica PRN code to play back early if it is positive and late if Δ is negative. One of the main goals of current GPS receiver research is developing an efficient technique for the receiver to accumulate I_{jk} and Q_{jk} in software. The Doppler shift is introduced here explicitly because it is assumed to be constant over the accumulation interval.

[37] The accumulations in equations (11) and (12), computed with a set of Δs, provide the means to track a GPS signal. In the simplest case, one uses Δ = 0, −1/4, and +1/4 chips to produce what are known as the prompt, early, and late in-phase and quadrature accumulations. These accumulations are used as input into the code and carrier tracking loops. For example, by computing the early and late accumulations, the receiver knows whether to advance or retard the $\hat{\tau}_{jk}$ to maximize $I_{jk}^2(0) + Q_{jk}^2(0)$.

[38] A simplified form of equations (11) and (12) for the prompt accumulations accumulated over 1 ms when the GPS receiver is sufficiently tracking the signals is

$$I_{jk}(0) \approx N_k A_j D_{jk} \cos\left(\Delta\phi_{jk}\right) + \eta_{Ijk} \quad (13)$$

$$Q_{jk}(0) \approx N_k A_j D_{jk} \sin\left(\Delta\phi_{jk}\right) + \eta_{Qjk} \quad (14)$$

where $\Delta\phi_{jk}$ is the change in the difference between the received signal's phase and the carrier replica's phase for the jth satellite over 1 ms and the noise terms η_{Ijk} and η_{Qjk} are assumed to be due to the product of the received signal's noise and the replica signals. A typical L1 C/A code receiver samples the received GPS signals at ~5 MHz, making $N_k \approx 5000$ for 1-ms accumulation intervals, although this varies among receivers.

[39] It is typical for a GPS receiver used for scintillation studies to output the power in the prompt accumulations at a rate of 50 Hz. This is accomplished by either coherently or noncoherently integrating the signals over 20 ms, which is the nominal length of the GPS data bits. Integration over shorter time periods is used for acquiring signals but for tracking signals, shorter integrations produce extra data that must be stored and postprocessed. Integration over time periods longer than 20 ms is not possible due to the bit transitions of the unknown data bits.

[40] In the noncoherently integrated case, the wideband power estimate of the signal is

$$WBP_{jl} = \sum_{k=k_l}^{k_l+20-1} I_{jk}(0)^2 + Q_{jk}(0)^2 \approx 20N_k^2A_j^2 + \eta_{IQjl} \quad (15)$$

where l is a nominal 20-ms sample time index. N_k corresponds to 1 ms of the GPS signal and the factor of 20 corresponds to 20 ms of integration. This result is primarily a function of received signal's power A_j^2, but also contains a cumulative noise term η_{IQjl}. A plot of the wideband power as a function of code shift ($\hat{\omega}_{Doppjk}$) and Doppler shift ($\hat{\tau}_{Doppler}$) is shown in Figure 3 for 1 ms integrations that would be used, for example, in acquiring GPS signals. The z-axis represents $I_{jk}^2(0) + Q_{jk}^2(0)$ and a clear peak is seen at the correct code shift and Doppler shift. The accumulation ($I_{jk}^2 + Q_{jk}^2$) scale is linear. One should note that the ratio of maximum accumulation compared to local maxima in the noise is

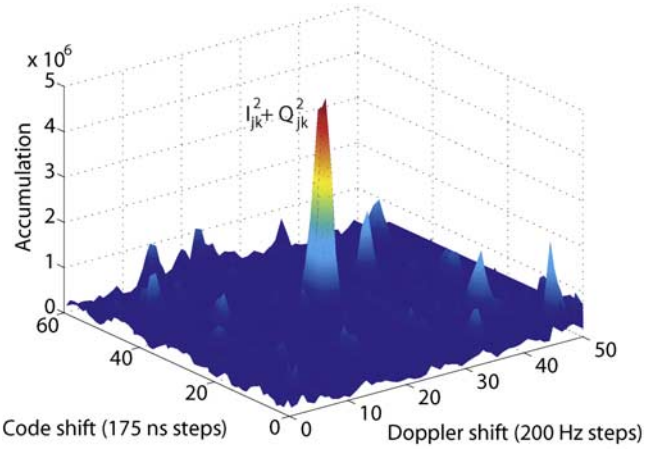

Figure 3. Accumulations ($I_{jk}^2 + Q_{jk}^2$) as a function of code shift, $\hat{\tau}_{jk}$, and Doppler shift, $\hat{\omega}_{Doppjk}$, estimates. The accumulation is performed over 1 ms of 5.7 Msample/s data. The peak at the center of the graph represents the signal from PRN27 at high elevation, $\simeq 75^\circ$.

only a ratio of 4–5 for this specific high elevation and strong signal GPS satellite, illustrating that GPS is a weak signal system. A relatively small decrease in amplitude yields a signal amplitude equal to the noise amplitude.

[41] The carrier-to-noise ratio, expressed in dB-Hz, can be computed from the wide-band power estimate using:

$$C/N_0 = 10\log_{10}\left[\left(WBP_{jl}/\eta_{lIQjl} - 1\right)50\right] \tag{16}$$

where the factor of 50 corresponds to the assumed 50 Hz accumulation rate. The carrier-to-noise ratio is frequently referred to as power when investigating GPS scintillations.

3.3. Code and Carrier Tracking

[42] As mentioned, the code and carrier components of the GPS L1 C/A code signal, namely the parameters that make up the C_j[] and the sin{} and cos{} terms, are tracked during normal receiver operation. The standard methods to track these components are with a delay-lock loop (DLL) to track the code and a frequency-lock loop (FLL) or phase-lock loop (PLL) to track the carrier signal. For a more elaborate explanation of tracking methods, see *Van Dierendonck* [1996].

[43] A DLL measures the movement of the code which primarily changes due to satellite and receiver motion. Carrier aiding uses the carrier Doppler shift output from the carrier tracking loop to guide the code tracking. The code tracking component of a GPS receiver tends to be quite robust when tracking scintillating signals. For this reason, DLLs will not be discussed further, and the interested reader can refer to *Van Dierendonck* [1996] for additional information.

[44] Carrier tracking is performed using either an FLL or a PLL. An FLL tracks the Doppler shift of the carrier signal, but does not track the phase of the carrier signal. FLLs tend to be fairly robust in terms of ability to maintain lock on a signal. Nevertheless, they are not well-suited for measuring phase scintillations or for dual-frequency GPS signal tracking, due to their inability to track the signal phase.

[45] A PLL tracks both the frequency and the phase of the received GPS signal. Tracking the signal phase is particularly important in scientific applications of GPS receivers. Precise estimates of signal phase are used for measuring phase scintillations. The signal phase is also used, along with the code range or pseudorange, to estimate the integrated electron density along the signal ray path. Otherwise known as the total electron content (equation (7)), this is a fundamental measurement of current data-driven ionospheric models [*Schunk*, 1995] and 3-D imaging techniques [*Bust et al.*, 2004].

[46] A large body of literature exists for Costas-type PLLs, which are commonly used in GPS receivers. These PLLs are used because they provide means to remove the phase transitions of the navigation data bits. Recall that the GPS signals are biphase shift-keyed (BPSK), which is a phase modulation scheme for encoding the navigation data bits. The data bits which appear as $\pm\pi$ transitions in the received signal phase, can occur nominally every 20 ms.

[47] A PLL can be adjusted to provide different loop bandwidths, accumulation intervals, and navigation data bit discriminators. Typical bandwidths are between 5 and 15 Hz. Common accumulation intervals are 1, 10, and 20 ms. An example of popular discriminators are the conventional Costas, arctangent, and decision-directed. Recent research into tailoring carrier tracking loops to be optimized for scintillations has provided insight into improved PLL design [*Van Dierendonck*, 1996; *Morrissey et al.*, 2002; *Humphreys et al.*, 2005].

[48] Scintillations appear as amplitude and phase fluctuations in the received GPS signal. In equation (8), the components that vary are A_j and ϕ_j. The tracking loops will see these variations as fluctuations in the sum of the squares of I_{jk} and Q_{jk}, which is related to C/N_0, and fluctuations in the phase, which is the rotation of the I_{jk} and Q_{jk}. The signal phase is related to the arctangent of the ratio of the quadrature accumulation to the in-phase accumulation. As the signal power becomes smaller, the accumulations also become smaller and move toward the origin in I-Q space. For a constant noise source, the relative impact on I_{jk} and Q_{jk} becomes larger for smaller signals and the phase exhibits large variations.

[49] *Humphreys et al.* [2005] describes a variable-bandwidth PLL designed to maintain lock during ionospheric scintillations. This Kalman filter-based PLL (KFPLL) models the phase dynamics due to satellite motion and the receiver clock. It also adjusts its effective loop bandwidth based on the estimated C/N_0. At high C/N_0 the

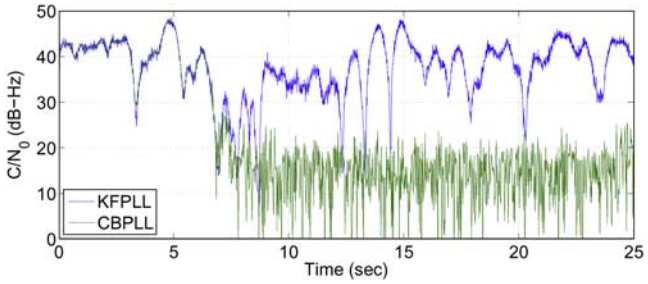

Figure 4. Tracking results comparing the Kalman-filter-based PLL and a 15-Hz constant-bandwidth PLL.

loop bandwidth is 15−20 Hz, but as C/N_0 decreases, the loop bandwidth decreases, allowing the KFPLL the ability to maintain lock on weaker signals. Weak signals tend to be dominated by noise, so it is important to decrease the loop bandwidth to decrease the contribution of noise to the estimate of the signal frequency and phase. Another approach to tracking weak signals is to increase the accumulation interval, but the data bit transitions typically limit this approach. This implementation of the KFPLL can maintain lock on signals that are ~7 dB weaker than a 15-Hz Costas constant-bandwidth PLL (CBPLL) with a decision-directed discriminator.

[50] *Humphreys et al.* [2005] recorded wide-band GPS L1 C/A code data sampled at 5.714 MHz. The data was collected in Cachoeira Paulista, Brazil in January 2003 near the southern equatorial anomaly during a period of strong ionospheric scintillations. This method of recording wide-band data, prior to correlation, provides a way to compare different tracking loops via postprocessing. Another advantage of having collected wide-band data is that it provides real data exhibiting scintillations, as opposed to simulated data.

[51] Figure 4 compares the tracking results of the KFPLL with a constant-bandwidth decision-directed Costas loop with a 15-Hz loop bandwidth. The KFPLL in blue maintains lock during the >20 dB deep fade. Reducing the constant-bandwidth loop's bandwidth to 10 Hz allows the loop to maintain lock through the fades. Nevertheless, the 10-Hz loop exhibits cycle slips as shown in Figure 5. The detrended carrier phase output from the KFPLL and the CBPLL are shown in Figure 5a. Figure 5b shows the difference between these detrended phases, which exhibits $\pm\pi$ jumps in relative phase. These jumps occur on the CBPLL, are nonphysical, and illustrate the occurrence of cycle slips.

[52] Reducing the constant-bandwidth PLL's bandwidth to 5 Hz allows it to maintain lock and prevents cycle slips. The disadvantage of using a constant 5-Hz PLL all the time is that fast phase fluctuations due to phase scintillations may be missed or undersampled. This is particularly an issue at auroral latitudes where amplitude scintillations are typically weak and phase scintillations dominate.

[53] Having collected data during scintillations produced another advantage over pure simulation, namely, a comprehensive understanding of why GPS receivers lose lock during scintillations. *Humphreys et al.* [2005] states that the deep signal power fades produce circumstances in which tracking the carrier phase of the GPS signal is essentially impossible, leading to loss of lock. This is in contrast to the previously held understanding that rapid phase fluctuations due to destructive interference are the cause of loss of lock. For this example, regardless of the amount of phase fluctuation during the deep power fades, the signals are simply too weak to maintain carrier lock. The general cause of loss of lock is more controversial and some investigators suggest that fast phase fluctuations can be the causal factor. One should note that power fades will not only cause loss of lock but also make signal acquisition more difficult.

3.4. Issues Regarding Dual-Frequency Signal Tracking

[54] In order to estimate the TEC along a satellite ray path, both the GPS L1 and L2 signals must be tracked. Current dual-frequency receivers track the L1/L2 P(Y) code using codeless or semicodeless techniques. These signals are tracked because the P(Y) code is the only L2 signal that the entire constellation broadcasts. Recently, an upgrade to the GPS constellation has begun. The upgrade will provide additional military signals on L1 and L2 along with a civilian-accessible signal on L2. This signal is known as L2C or the L2 CM/CL signal. Currently, three satellites broadcast this signal, although more upgraded GPS satellites will be launched frequently, and within several years, the entire constellation will be upgraded.

[55] Typical codeless techniques involve auto or cross-correlation of the two received P(Y) code signals. This process degrades the ability to track weak signals significantly. Semicodeless techniques, which are improvements over codeless techniques, correlate the received signals with the unencrypted P code, typically at a fast accumulation rate. A fast accumulation rate is needed because of the unknown encrypting W bits. The best semicodeless tracking method is called Z-tracking. This method correlates the incoming L1 and L2 signals with the unencrypted P code at a fast accumulation rate, typically around 480 kHz. The accumulations are then low pass filtered producing reasonable estimates of the encrypting W bits, which aid in the signal correlation. The use of a fast accumulation rate increases what is known as squaring loss, degrading performance of receivers that use this technique.

[56] The optimal way to track dual-frequency GPS signals is by coded tracking which is straightforward for unencrypted, civilian-accessible signals. Figure 6 compares the performance of semicodeless tracking to coded tracking. The figure shows the output PLL signal-to-noise ratio (SNR) as a function of the input GPS signal strength in units of dB-Hz. The output PLL SNR depends on both

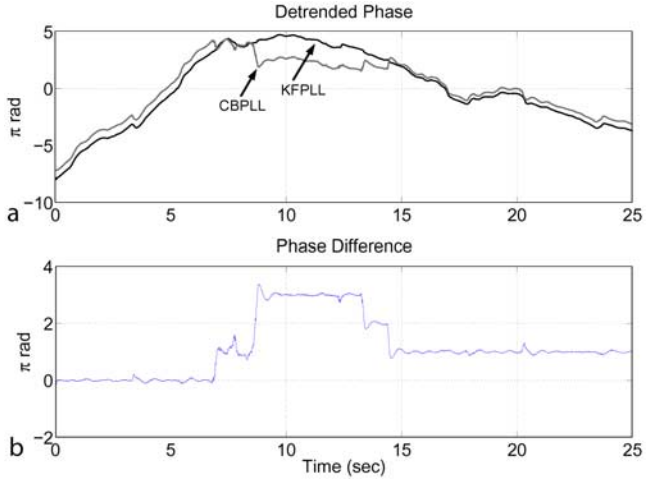

Figure 5. Detrended signal phase from the KFPLL and a 10-Hz CBPLL.

C/N_0 and the bandwidth, on whether there is a squaring loss, and on the order and tuning of the loop. Roughly speaking, if there is no squaring loss, then SNR = $(C/N_0)/B$, where C/N_0 is in absolute Hz units and B is the bandwidth in Hz [*Proakis*, 2001]. This is done for three different accumulation rates of 480 kHz, 50 Hz, and 0 Hz. The first represents semicodeless tracking, the second coded tracking of a signal with data bits modulated at 50 Hz (e.g., the L1 C/A code, L2 CM code, or the military P code), and the last accumulation rate represents the theoretical limit, assuming that the data bits are known. The main decrease in SNR as seen by the PLL is due to squaring loss, which is linearly proportional to the accumulation rate. Coded tracking with the 50-Hz accumulation rate beats out semicodeless tracking by nearly 20 dB.

[57] For scintillating signals, which become weak at times and may exhibit large and rapid phase dynamics, the use of coded tracking becomes absolutely necessary in order to maintain signal lock. This is particularly important during deep fades, when the physics of the scintillations is most interesting and least understood. It is also important in order to produce TEC estimates, which requires simultaneous tracking of the two signals.

[58] Two issues are worth mentioning in regard to maintaining lock concurrently on two signals. First, the signals broadcast from GPS satellites can be at different power levels. For example, the L2 signals are weaker than the L1 signals and the new L2C signal is 1.5 dB weaker than the L1 C/A code signal. This will make tracking the L2 signal more difficult in a scintillating environment.

[59] Second, the scintillation-inducing effects of the irregularities are dependent on the frequency of the incident signal. In the simple single-scattering case the phase deviation induced by the irregularities is inversely proportional to the signal frequency. In addition, the longer Fresnel length of the lower frequency signals typically corresponds to larger power spectral densities within the irregularities. Thus lower frequency signals are more strongly affected than higher frequency signals, which is well known [*Yeh and Liu*, 1982].

[60] The authors are unaware of any published results showing separate GPS L1 and L2 amplitude scintillations. It is expected from the relative closeness in Fresnel scales sizes of the L1 and L2 signals, where the ratio of Fresnel scales of L1 to L2 is the square root of the ratio of their respective wavelengths (0.88), that the amplitude scintillation time histories for received L1 and L2 signals will be similar. The only difference may be the peak-to-peak magnitude of the signal power variations will be larger on the L2 signal by the ratio of the L2 to the L1 wavelengths, or about 2–3 dB.

3.5. Issues Regarding Acquisition

[61] Before a GPS satellite signal can be tracked, it must first be acquired. Acquisition typically consists of four steps referred to as code, carrier, bit, and frame. Code and carrier are acquired simultaneously by searching both code shift and Doppler shift space. This can either be done through a brute force approach of searching through all possible code shifts whose increment must be smaller than a code chip (997.5 ns) and over Doppler bins of about 200 Hz compared to the possible Doppler shift space of ±5 kHz. An alternate method is to use a Fourier transform approach. Figure 3 shows the results of a brute force approach to finding the signal as an $I^2 + Q^2$ peak in code shift/Doppler shift space. The next step is to detect the existence of bit transitions, which occur every 20 ms as the carrier phase changes by π when the bit value changes. The bits are arranged in subframes of 300 bits, and five subframes make a full frame. The entire GPS navigation message is broadcast over 25 frames, taking 12.5 min, although for navigation, only subframes 1–3 of any frame are required. Frame lock occurs when an 8 bit preamble to each subframe within a frame is detected. The first three subframes of each frame contain the satellite clock offset and ephemerides for determining the satellite position. Also, each subframe contains six parity bits but no forward error correction.

[62] In a scintillating environment one expects frequent power fades with typical timescales of a fraction of a second to a few seconds (see section 4.2). For code and carrier acquisition, a fade could occur at just the wrong moment during a brute force acquisition or for the data sample (typically a few ms) used in the Fourier transform approach. The only mitigation to this danger is to continue the acquisition process, which most GPS receivers do with spare channels not tracking. Bit acquisition is a process that typically examines several seconds of signal looking for systematic phase transitions. Since this process creates averages over times at the upper range of typical fade durations, it is likely that bit acquisition is only affected in unusual conditions.

[63] Currently the fastest sampling GPS scintillation receivers calculate power every 20 ms corresponding to

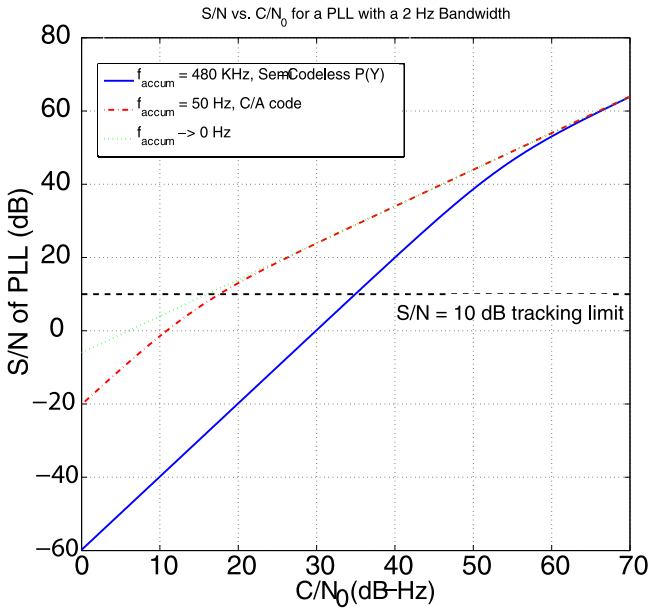

Figure 6. Comparison of tracking capabilities of semicodeless and coded techniques.

a bit length. As far as we know, no one has examined GPS bit error rates in a scintillating environment. Scintillations could therefore be a significant source of false bit transitions, which could lead to failure in finding the subframe preambles or to false data that are critical to navigation. The latter would likely be detected by subframe parity bits. However, since the subframe is transmitted over 6 s and only one false bit transition is required to make the entire subframe suspect, it is conceivable that frame lock may not occur until the signal stops scintillating. Introduction of false data is unlikely because of the parity bits that are required to interpret the navigation message.

[64] Reacquiring a signal after loss of lock is not as problematic as acquisition since the satellite clock offset and ephemerides are valid for 2 to 4 hours. Stored values for these parameters can be used during the scintillation period. Furthermore, during reacquisition the region of code shift and Doppler shift space that must be searched can be greatly reduced by knowing the values before loss of lock. Nonetheless, the preambles must be correctly interpreted to obtain valid pseudoranges.

[65] Overall the issue of acquisition within a scintillating environment has received little attention within the space weather community. With currently available GPS signal simulators and digital storage receivers, the effect of scintillations on various acquisition strategies can be analyzed and should be a goal of current research.

4. GPS Scintillations at Low Latitudes

[66] GPS scintillations at low latitudes are primarily associated with equatorial spread *F*. Spread *F* is a descriptive name whereby the reflected signals recorded by an ionogram cease forming distinct time-of-delay-versus-frequency traces and instead exhibit a spread in frequency within the ionospheric *F* region, which is caused by scattering from ionospheric irregularities. Equatorial spread *F* refers to spread *F* at the magnetic equator up to about ±15° latitude, which includes the higher density anomalies (discussed in section 4.3). Observations of equatorial spread *F* began as early as 1938 [*Booker and Wells*, 1938] and the investigation of this subject is much too broad to be reviewed or even summarized here. For our purposes we simply note that equatorial spread *F* is caused by ionospheric irregularities with a spatial spectrum extending from 100 km to less than 1 m. These irregularities cause scintillations at least up to 7 GHz [*Aarons et al.*, 1983].

[67] Equatorial spread *F* develops shortly after sunset and propagates both upward and to off-equatorial latitudes in the electromagnetic equivalent of the Rayleigh-Taylor instability [*Anderson and Haerendel*, 1979]. As the lower density ionosphere moves upward into the higher density ionosphere, it creates a hole, sometimes called a bubble. Velocity shear mixing within the hole gradients, along with the formation of drift waves, create most of the ionospheric density irregularities [*Kelley*, 1985]. After the hole develops and rises into the topside *F* region ionosphere, it typically stops evolving and the structure is "frozen" into the moving ionosphere. As the night progresses, diffusion causes the irregularities to decay starting with the shortest scale lengths. At sunrise, solar ionization refills the flux tube and the irregularities disappear at all wavelengths. Geomagnetic activity can change this progression of events, usually suppressing the onset of equatorial spread *F* before local midnight and initiating it after midnight [*Rastogi and Kroehl*, 1978].

4.1. Relation of Scintillations to Equatorial Spread *F* Bubbles

[68] As noted earlier, ionospheric irregularities at the Fresnel length produce scintillations if the ionosphere is sufficiently dense and the density depletions within the irregularities are sufficiently intense (equations (3) and (4)). Since irregularities are produced in equatorial spread *F* bubbles, GPS scintillations should be produced when the signals encounter the bubbles. Figure 7 shows two examples where GPS signals encounter depletions in the ionospheric TEC (Figure 7c) and amplitude (diffractive) scintillations are observed in the GPS signals (Figure 7b). The power (C/N_0) in PRN 14 is typical of a GPS pass. The power increases as the satellite rises from the western horizon primarily because the receiving antenna gain increases at higher elevations. As the satellite sets to the east, the signal power decreases in response to the receiving antenna gain dependence on elevation. The TEC depletion between 2200 and 2300 UT is evidence of a bubble, and the signal power fluctuations to higher and lower power (amplitude scintillations) are coincident with

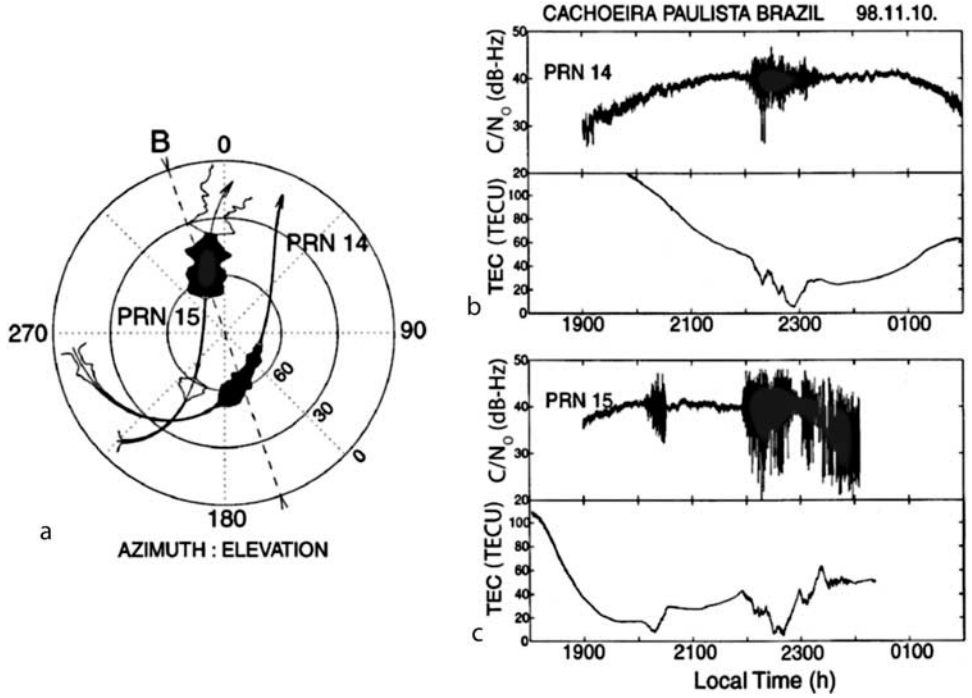

Figure 7. Example of equatorial bubbles producing rapid amplitude fluctuations in GPS signals (diffractive scintillations), showing (a) the elevation-azimuth trajectories of PRN 14 and PRN 15. The width of the envelope corresponds to the value of the S_4 index. The times between 2200 UT and 2400 UT have been filled. Also shown are (b) the GPS L1 signal power for each signal and (c) TEC.

the bubble. PRN 15 is somewhat different in that it encounters more bubbles but the relation between amplitude scintillations and the depletions in TEC is still one-to-one.

[69] Figure 7a shows the elevation-azimuth trajectories of PRN 14 and 15 with the width of the line being proportional to the scintillation S_4 value and the dashed line being the magnetic meridian. The times between 2200 UT and 2300 UT have been filled in. In this case when the two satellite signal ionospheric puncture points are aligned on the same magnetic meridian (dashed line), they respond to irregularities in a spread *F* bubble also aligned along the magnetic meridian. Conversely, other times do not exhibit the same correspondence because of the limited southward extent of the bubbles, which implies limited vertical extent at the equator. This event was recorded at Cachoeira Paulista, Brazil under the southern equatorial anomaly.

[70] The event in Figure 7 illustrates some of the features of equatorial spread *F* irregularities and scintillations at the equatorial anomaly. First, the onset of the scintillations is typically 1 to 2 hours after sunset. The irregularities begin after sunset at the equator (about 1900 LT), rising vertically, extending poleward, and reaching the anomalies a few hours later. The regions of the sky in which irregularities occur can also be variably distributed. The signal from PRN 14 experiences only a brief period of scintillations whereas the signal from PRN 15 scintillates for nearly half of its pass because the bubbles do not always extend sufficiently poleward for the southernmost satellite (PRN 14) to experience scintillations. The scintillations do not typically have maximum amplitudes inside the bubble but are stronger on the bubble TEC gradients or just adjacent to the TEC bubble. Signal paths that encounter irregularities may not be optimal for observing minimal TEC.

[71] The examples in Figure 7 illustrate isolated regions of scintillations, which is not always the case. Figure 8 is an example in which virtually all of the GPS satellites in the upward hemisphere are scintillating. In this example S_4 is plotted for the period of 2200–2400 LT for six satellites and four receivers located in Brazil at Manaus (3.1°S, 60.0°W), Cuiabá (15.6°S, 56.0W), Cachoeira Paulista (22.7°S, 45.0W) and São José dos Campos (23.2°S, 45.9W). An example of undisturbed signal can be seen for São José dos Campos, PRN 27 or 28 at 2315. Despite these brief periods of quiet, there are several times when all satellites are scintillating. For example, at both Manaus and Cuiabá all of the satellites are continuously scintillating over the 2-hour period. Not shown are an additional six satellites seen by two or fewer receivers for only a fraction of the 2-hour period. All of these satellite signals were

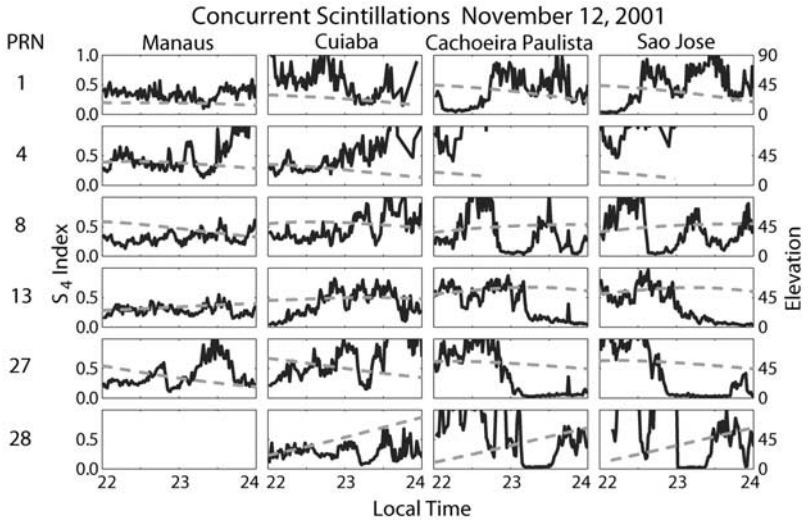

Figure 8. GPS S_4 observations at four sites distributed over Brazil.

scintillating when observed between 2200 and 2400 LT. From the GPS receiver viewpoint, irregularities may be distributed over the entire equatorial sky for at least 2-hour durations.

4.2. Temporal Scales of Scintillations

[72] In addition to knowing when and where scintillations occur at low latitudes and how strong they are, the temporal scales or fade times of the amplitude fluctuations are important to understanding how GPS receivers respond. The temporal scales will determine, in part, how the GPS receiver tracking loops respond, as described in section 3.3. Temporal scales are examined in Figure 9, which shows another example of GPS scintillations measured within the equatorial anomalies [*Kil et al.*, 2000]. The signal from PRN 15 is shown for an event 2 days earlier than that in Figure 7 and so it had virtually the same elevation-azimuth trajectory as shown in Figure 7a. In Figure 9 the signal from PRN 15 scintillates for 2/3 of the pass. In Figures 9a and 9b and Figure 9e, the relation between scintillations and equatorial bubbles is reconfirmed. The Figure 9b is the S_4 index. Again, scintillations as evidenced by a fluctuating amplitude (Figure 9a) or the S_4 index (Figure 9b) were collocated with regions of ionospheric TEC gradients.

[73] In this particular experiment, four spaced GPS scintillation receivers were employed so that drift velocities could also be measured. In Figure 9d, two estimates of velocity are plotted. The circles represent the estimated ionospheric irregularity drift velocity calculated from the measurement of scintillation pattern drift velocity on the ground using the magnetically east-west-spaced GPS receivers. The solid line represents the estimate of the velocity on the ground of a projection of the magnetic field along the GPS satellite signal path and this projection moves because the GPS signal ionospheric puncture point is moving. The projection starts at the satellite and is assumed to intersect irregularities at 350 km altitude corresponding to the assumed irregularity height. This can be thought of as the scintillation drift speed on the ground that would occur if the ionospheric irregularity velocity were zero (B. M. Ledvina et al., Ionospheric scattering altitude estimation using closely spaced GPS receivers, submitted to Radio Science, 2007). When the two speeds are equal (near 2300 UT), they cancel each other so that the scintillation pattern drift velocity is small.

[74] The rapid fluctuations of the GPS signal amplitude are sometimes referred to as fading. An important property of fading is its temporal scale, which is roughly given by the Fresnel length divided by the scintillation pattern velocity. To represent the fading timescale statistically, the normalized autocorrelation function of the signal amplitude is created and the 3 dB width is calculated (i.e., the width of the autocorrelation function at half maximum) for a sample 40 s long. The result is shown in Figure 9c. For most of this pass the characteristic timescale is about 1 s but near 2300 UT the timescale increases dramatically to more than 4 s. The time at which the fading timescale is a maximum corresponds to the time at which the irregularity speed and the projected magnetic field speed match each other. That is, the ionospheric irregularity speed moving the scintillation pattern from west to east is cancelled by the motion of the projected magnetic field line from east to west (velocity matching or resonance). At this time the scintillation pattern drift speed slows down and the fading timescale increases.

[75] The first examples of velocity matching were reported at VHF frequencies using an airborne receiver [*Aarons et al.*, 1980a]. This result seems to have been overlooked until recently. Analysis and modeling of scintillations neglected the effect of velocity matching on scintillation [e.g., *Fremouw et al.*, 1980; *Rino and Owen*,

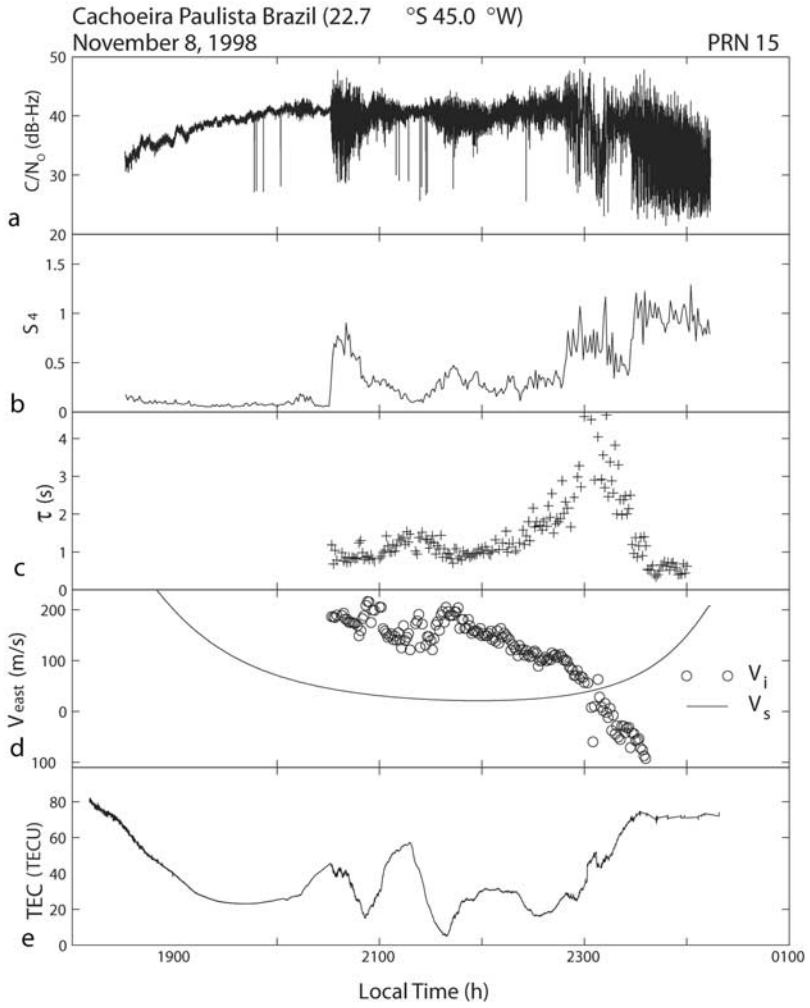

Figure 9. Example of diffractive scintillations with a variable timescale. See text. (After *Kintner et al.* [2001].)

1984; *Fremouw and Secan*, 1984]. The International Telecommunication Union-Radio Communications sector also seems to have overlooked fade stretching in their recommendation on ionospheric propagation (ITU-R P.531-6). These oversights cannot be corrected by a simple linear transformation since the fading timescale is determined by the relative velocity of the scintillation fade pattern, the evolution of the irregularities within the ionospheric reference frame, and by the GPS signal path angle of incidence, which is continuously changing.

[76] The significance of longer fade times is that the GPS receiver tracking loops are more likely to fail at low signal amplitudes if the fading timescales are longer. For equally low signal amplitudes but with short fading timescales, the receiver tracking loops ''free wheel'' through the fades.

[77] Figure 10 shows an example of the effect of longer fading time scales on the ability of a GPS receiver to track. Figure 10 is a 2-min record of the signal amplitude during the period (shown in Figure 9) when the fading timescales were the longest, just after 2300 UT. Three examples of loss of lock (indicated by the arrows and shown as straight lines) with timescales varying from 1.5 s to 6 s occurred. These examples are relatively minor since none of them exceeded 10 s. In severe cases the loss of lock can exceed several tens of seconds. One should note that the velocity matching to produce longer fading timescales also depends on the receiver velocity and the size and shape of the scintillation pattern [*Kintner et al.*, 2004]. In general, velocity matching is more likely to occur for receivers moving west to east with velocities of about 100 m/s, which corresponds to aircraft speeds [*Kintner et al.*, 2001].

[78] The duration of GPS signal fade caused by destructive, diffractive interference in the moving reference frame of the scintillation pattern has rarely been addressed. This would be the maximum length of time that a fade could last in the resonant reference frame. One experiment to address this question was performed in Cachoeira, Brazil with three GPS receivers spaced in an east-west direction

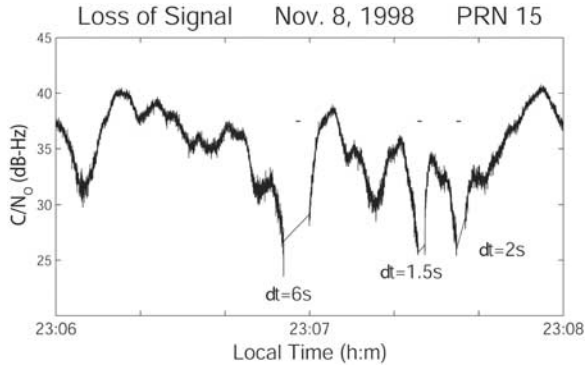

Figure 10. Example of loss of lock on a GPS signal with long timescale scintillations. The data were obtained at Cachoeira Paulista, Brazil under the southern equatorial anomaly.

at locations 0 m, 218 m, and 715 m. Normalized cross-correlations of the amplitude scintillation patterns from each antenna were then created as a measure of how much the scintillation pattern changes in moving between the various antennas. The normalized cross-correlation yielded a lag time of optimal correlation and value for the optimal correlation. Depending on the scintillation pattern speed and antenna separation (218 m, 487 m, or 715 m) a variety of times were sampled. Over 30,000 normalized cross-correlations were created for situations in which $S_4 > 0.5$ and the result is plotted in Figure 11 as density surfaces. The full results can be found in the work of *Kintner et al.* [2004].

[79] Figure 11 shows as equal density surfaces the log of the number of events that occurred in 0.5 s by 0.02 optimal correlation amplitude bins. For example, the bins at the shortest times (near 0 s) were populated by cross-correlation amplitudes in which the scintillation patterns moved most rapidly over the shortest receiver separation. Since the nighttime ionosphere primarily moves from west to east, most cross-correlation samples were for positive lag times. For lag times that are more positive or more negative, the cross-correlation amplitude decreases as the scintillation pattern evolves in time. By examining the decrease in cross-correlation amplitude, a measure of how much the scintillation pattern evolves can be obtained. For example, at a 5 s positive lag time, 34% of the events have a cross-correlation amplitude of 0.85 or larger, suggesting that for a receiver in resonance with the scintillation pattern, about one-third of the fades will have a lifetime of at least 5 s. Even for a lag time of 10 s, events exceeding the cross-correlation amplitude threshold of 0.85 exist. Fades of this length will not only cause loss of lock, if sufficiently deep, but will also make reacquisition problematic as well. This effect can be seen in Figure 4 of *de Rezende et al.* [2007] in which tracked satellites were lost and tracking did not resume for several minutes.

4.3. Equatorial Scintillation Morphology

[80] The morphology of equatorial scintillations is characterized by two timescales and a spatial distribution. The first timescale is the 11-year solar sunspot cycle and the second timescale is a seasonal or annual dependence. The spatial distribution is dominated by the location of the largest ionospheric densities, which are the equatorial anomalies, about 15 degrees from the magnetic equator.

[81] Figure 12 shows the frequency of scintillations measured from São José dos Campos, Brazil at about 13 degrees S. magnetic latitude, during the period leading to the solar cycle 23 maximum in 2000. In Figure 12a both the percent frequency of $S_4 > 0.2$ and $S_4 > 0.5$ during darkness are shown for June 1997 to June 2002. Figure 12b shows the 10.7 cm radio flux (F10.7) as a proxy for the solar EUV intensity. The general trend for F10.7 is increasing during this period as is the occurrence frequency of both weak and strong scintillations. In addition, the scintillations show a seasonal dependence with a maximum in December-January and a minimum near May-June, which is characteristic of the Brazilian sector where magnetic north is about 13 degrees west of geodetic north. The sunset terminator will align itself most closely with a magnetic meridian during the December-January period, leading to this seasonal maximum [*Tsunoda*, 1985]. At other longitudes the sunset terminator will most closely align itself with the magnetic meridian at the equinoxes, leading to seasonal maxima in the fall and spring.

[82] The locations of the maximum equatorial scintillation amplitudes are not at the magnetic equator [*Aarons*, 1982] but instead are about 15 degrees on either side of the magnetic equator where the Appleton anomalies or equatorial anomaly crests are located. These crests are formed during the daytime when solar heating of the thermo-

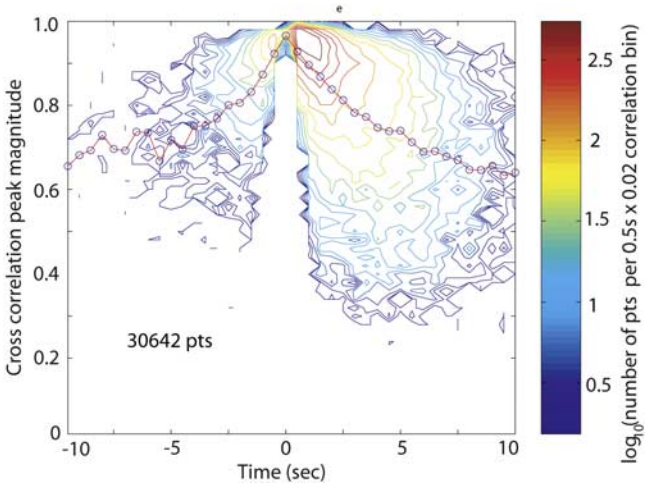

Figure 11. Log number of events in 0.5 s by 0.02 cross-correlation bin as a function of optimal lag time and optimal cross-correlation value. (After *Kintner et al.* [2004].)

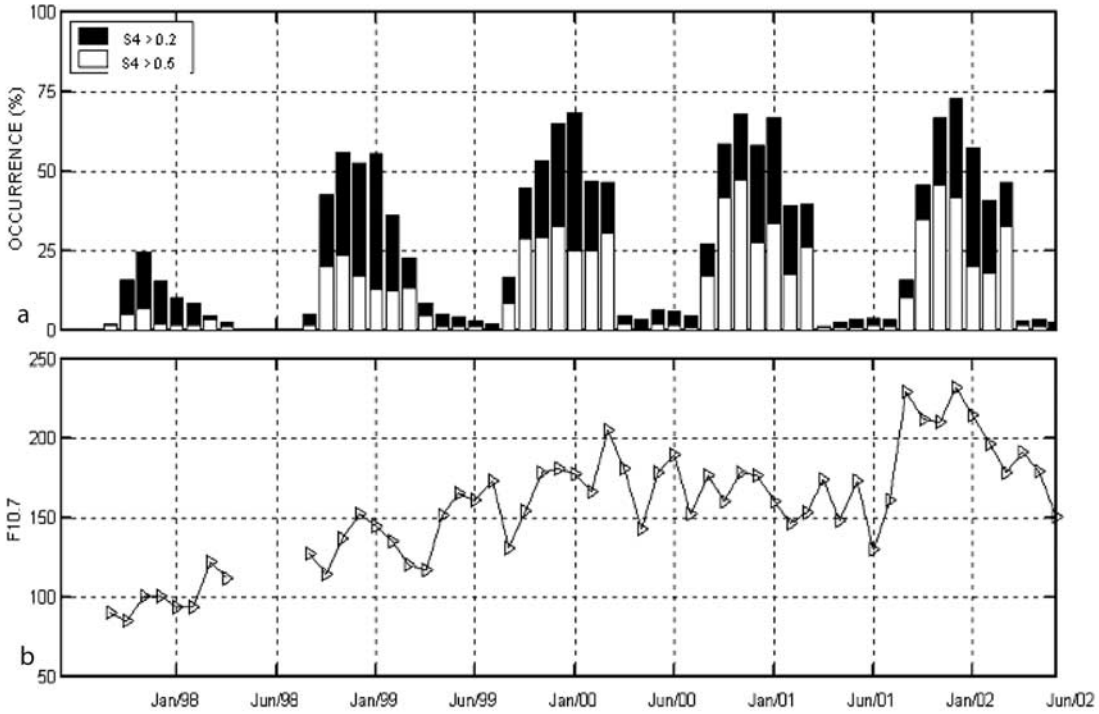

Figure 12. The dependence of weak ($S_4 > 0.2$) and strong ($S_4 > 0.5$) GPS amplitude scintillations on F10.7 and season at São José dos Campos, Brazil. (After *Rodrigues* [2003]. Reproduced by permission of INPE.)

sphere drives an eastward dynamo electric field. The electric field drives an upward flux of ionization at the equator, which subsequently falls down magnetic field lines at more polar locations, increasing the ionization density in two bands called the equatorial or Appleton anomalies. The enhanced ionospheric densities remain through darkness depending on the altitude and recombination rate. Also, the anomalies may not be symmetrical depending on the thermospheric winds. Equatorial bubbles initiated shortly after sunset rise at a few to several hundred meters/s and the flux tubes associated with these bubbles map to more poleward latitudes as the bubbles rise. When the stirring motions associated with the bubble turbulence reach the anomaly crests, they produce the most intense density irregularities.

[83] Although this feature was generally understood on a statistical basis from data collected in separate experiments, the existence of increased scintillation amplitude in the anomaly crest on a single night was demonstrated only recently. Figure 13 shows scintillations measured from eight GPS scintillation receivers spaced over eastern and central Brazil. The arc locations show the 350 km ionospheric puncture points (IPP) of the GPS satellite signals and the intensity of the scintillations is shown as a color-coded S_4 index. The coordinates are geodetic and the magnetic equator as well as the 25 degree dip latitude are shown as dashed lines from the southwest to the northeast. All of the measurements during the 6 hour period of 2100–2700 UT are shown for 17 March 2003. At the southern anomaly crest, about 15 degrees dip latitude, the S_4 index is clearly larger. The observation of similar scintillation behavior at the northern anomaly crest must await the deployment of more GPS scintillation receivers. With a larger range and greater density of GPS scintillation receivers, it will be possible to characterize the time evolution as well as the spatial distribution of scintillations.

5. GPS Scintillations at Midlatitudes

5.1. Introduction

[84] The definition of midlatitude is somewhat arbitrary. The effects associated with equatorial spread *F* have certainly been observed to move poleward beyond the equatorial anomalies and produce GPS scintillations in locations such as Hawaii [*Kelley et al.*, 2002], and during magnetic storms there appears to be extended activity from the anomalies poleward as the storm evolves [*Makela et al.*, 2001] in locations such as Puerto Rico. For this paper the definition of midlatitude will be somewhat conservative, referring to regions that are clearly decoupled from equatorial phenomena.

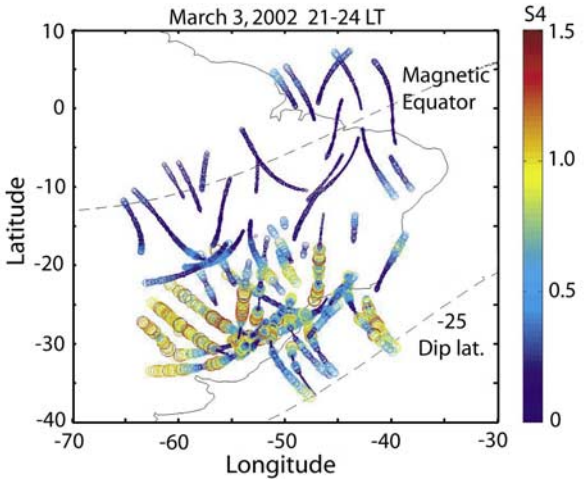

Figure 13. S_4 measured by GPS amplitude scintillations over Brazil during a single night. The equatorial anomaly is apparent in the larger S_4 values. (After *Rodrigues* [2003]. Reproduced by permission of INPE.)

[85] Midlatitude GPS scintillations have been investigated less often compared to low-latitude scintillations. The reason is quite simple. GPS scintillations occur much less often at midlatitudes and usually only in association with magnetic storms near solar maximum. Consequently, fewer observational resources have been dedicated to understanding the morphology and characteristics of midlatitude scintillations. With fewer resources committed, the probability of observation becomes even smaller.

[86] The principal source of data for understanding midlatitude scintillations comes from the National Geodetic Service (NGS) and the Continuously Operating Reference Stations (CORS) network of dual-frequency GPS receivers. The principal evidence for the presence of scintillations is the qualitative finding that dual-frequency tracking fails [*Skone*, 2001], as discussed in section 3.4. The quantitative explanation is more difficult, given the variety of receiver designs and lack of clear standards concerning their response to scintillations. These failures occur during magnetic storms and appear to be associated with two phenomena [*Basu et al.*, 2005]: either the equatorward movement of the northern lights over midlatitudes [*Basu et al.*, 2001; *Sojka et al.*, 2004], which is typically a nighttime phenomenon, or in association with storm-time ionospheric phenomena that do not involve particle precipitation. This latter set of phenomena is referred to with a variety of descriptive names, such as storm enhanced density (SED) and subauroral polarization streams (SAPS). The effect of this latter set of phenomena on GPS receivers through scintillations appears to be primarily in the daytime, suggesting that solar ionization is an important factor.

5.2. GPS Diffractive Scintillations at Midlatitudes

[87] The existence of diffractive scintillations at midlatitudes has been established at VHF/UHF frequencies during large magnetic storms [*Basu et al.*, 2001]. Very few fast sampling GPS receivers, which are adequate to directly measure diffractive scintillations, operate at midlatitudes, although on a few fortuitous occasions there has been some success. On one occasion GPS amplitude scintillations in association with a large magnetic storm, Dst = −387 nT, and with simultaneous observations of the northern lights produced an S_4 = 0.18 at Bear Lake, Utah [*Sojka et al.*, 2004]. Other observations of midlatitude GPS scintillations have been in substantially smaller magnetic storms.

[88] Such an example was presented by *Ledvina et al.* [2002]. Figure 14 shows an example of GPS scintillations in which the peak value of S_4 was 0.8. Figure 14a shows Dst where there is evidence of a minor magnetic storm with a main phase value of about −100 nT. The shaded time span in Figure 14a is expanded over a shorter time interval in Figures 14b and 14c. Figure 14b shows the signal strength for a GPS satellite signal and Figure 14c shows the total electron content (TEC) for the same signal path. The signal strength began at nearly constant amplitude with slow, small changes due to multipath reflections near the antenna. At about 2400 UT the signals began to fluctuate rapidly with both positive and negative excursions that slowly diminished with time until the signal was lost near 2730 (0330) UT. The fluctuations were diffractive scintillations. Figure 14c starts with TEC values that were roughly double the nominal values and changed suddenly near 2400 UT when the scintillations began. The largest scintillations corresponded to the large TEC gradients, at which point the S_4 values reached a maximum of 0.8. Toward the end of the record the TEC increased rapidly as a result of low satellite elevation and longer slant path.

[89] The measurements of Figure 14 were made with a single GPS scintillation receiver so that drift measurements cannot be obtained directly. Instead, speed estimates can be obtained by analyzing the temporal scales of the scintillation amplitude fluctuations [*Kintner et al.*, 2001]. Using this technique, *Ledvina et al.* [2004] demonstrated drift speeds of 20–600 m/s. Such a large drift speed and such a large range of drift speeds suggests that the scintillations in Figure 14 were at least partially associated with the fast ionospheric drifts in subauroral polarization streams (SAPS) [*Foster and Vo*, 2002].

[90] The consequences of the midlatitude scintillations shown in Figure 14 can be seen in an expanded plot of the signal amplitude fluctuations present in Figure 15. Figure 15a shows the amplitude fluctuations presented in Figure 14 while Figure 15b shows the expanded timescale. During the period of the largest amplitude signal fluctuations, the GPS receiver experienced several periods of loss of lock or failure to track for up to 15 s at a time. These failures to track typically lead to increased dilu-

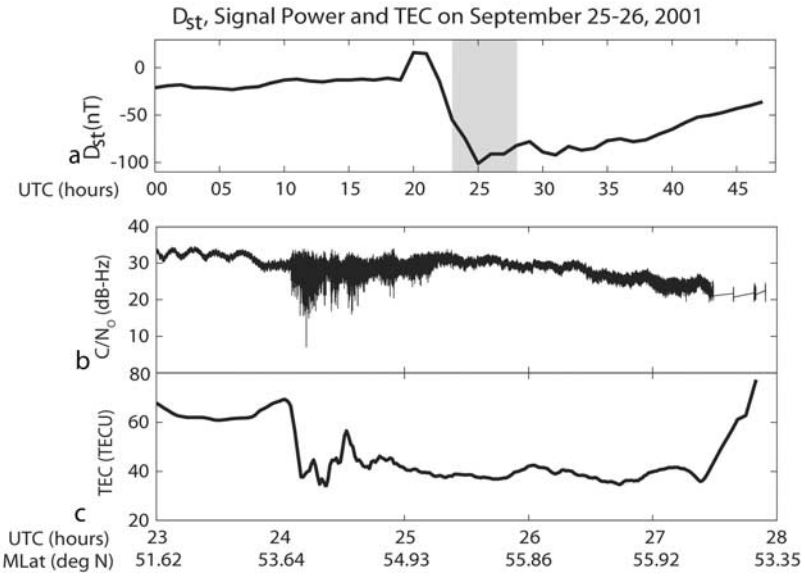

Figure 14. An example of (b) GPS signal scintillations coincident with (c) TEC gradients and (a) a minor magnetic storm. The GPS data were obtained at Ithaca, NY, USA. Note the difference in timescales between Figure 14a and Figures 14b and 14c. (After *Ledvina et al.* [2002].)

tion of precision, larger errors, and potentially failure to navigate.

[91] Other examples of midlatitude diffractive scintillations have been reported in Japan during the onset of magnetic storms. K. Ohshima (personal communication, 2005) reports many occurrences of scintillations in Japan over a 2-year period. These occur primarily during magnetic storms, but some of them are associated with other phenomena, such as traveling ionospheric disturbances (TIDs). The S_4 indices varied from 0.2 to 1.2, including loss of lock in both the TEC receivers and the GPS scintillation receivers. The larger amplitude S_4 values corresponded to a minor magnetic storm (Dst = −100 nT) similar to that shown in Figure 14.

[92] Additional analysis of these events is possible using the large number of dual-frequency GPS TEC receivers in Japan (>1000), which permits imaging of the ionospheric TEC. These images show that, in one of the two cases of scintillations, there were large-amplitude (TEC = 5–35 TECU), long-wavelength (100 km) structures that were aligned northwest to southeast and propagated toward the southwest at speeds of roughly 250 m/s. Similar structures have been observed by *Kelley et al.* [2000] with optical imaging at 630.0 nm in Puerto Rico. In addition, *Foster et al.* [2004] have observed similar periodicities in the flow velocities associated with SAPS. Together these observations point to a new and not understood ionospheric phenomenon that exists at midlatitudes and that produces ionospheric irregularities leading to diffractive GPS scintillations. These observations have offered a regional viewpoint which occasionally is at the right place at the right time.

5.3. Causes of Midlatitude Irregularities Leading to L-Band Scintillations

[93] The causes of midlatitude *F* region irregularities fall into two classes. The storm-time inner-magnetospheric electric field creating irregularities on preexisting ionospheric density gradients and local instabilities operating on preexisting ionospheric density gradients. How the preexisting gradients are produced initially is an equally compelling question, although there seems little doubt that during magnetic storms large regions hosting an ionospheric density gradient exist over North America and perhaps elsewhere [*Coster et al.*, 2005]. Incoherent scatter radar observations have demonstrated that these density gradients are associated with high velocity ionospheric flows, sometimes called subauroral polarization streams (SAPS), and with storm-enhanced densities (SEDs).

[94] Inner-magnetospheric electric fields have been confirmed from observations by DMSP satellites at about 800 km altitude, which reveal rapidly fluctuating plasma drifts, magnetic fields, and ionospheric densities in SAPS and regions of precipitating ring current ions. The Poynting vectors are both upwards and downward and in some cases the electric field and density fluctuations are coherent. *Mishin et al.* [2003a] suggest magnetoionosphere coupling as field-aligned currents (FAC) flow in regions of irregular density to maintain charge neutrality. Alfvén waves carry away charge imbalances and try to restore equilibrium by rearranging the potential pattern. However, the authors also suggest the electromagnetic O^+ cyclotron waves in the storm-time ring current may also be responsible for some of the more irregular observations. Simulta-

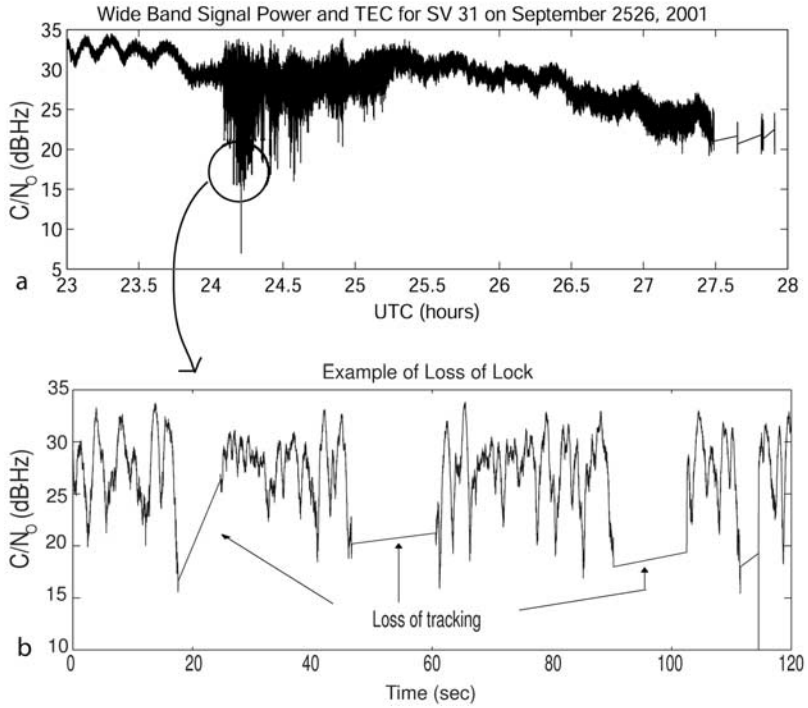

Figure 15. (a) GPS signal power showing fluctuations produced by diffractive scintillations from Figure 14b and (b) expanded timescale of GPS signal power showing loss of tracking.

neous DMSP observations of rapidly fluctuating plasma drifts were demonstrated to be near the observations shown in Figure 14 [*Mishin et al.*, 2003b].

[95] Other authors suggest a local origin on the trough wall region from the ion temperature gradient convective instability in association with the gradient-drift instability or from an ion frictional heating instability [*Keskinen et al.*, 2004]. The measurements in Figure 14 support this view in part because the largest amplitude scintillations occur on the edge of steep density gradient leading to a region of smaller and more variable TEC. The density gradient is typical of that expected for the trough wall.

[96] Finally, the $E \times B$ instability is also a candidate for producing Fresnel scale irregularities. K. Ohshima (personal communication, 2005) suggests that the density gradients observed in their TEC images are unstable to dynamo electric fields driven by neutral winds. Since their observations demonstrated multiple ridges of TEC with gradients on both the leading and trailing edges almost any neutral wind, except those parallel to the ridges, would excite the $E \times B$ instability.

6. GPS Scintillations at High Latitudes

[97] Scintillations at high latitudes have been investigated extensively at VHF and UHF frequencies. Intense diffractive scintillations have been observed by *Basu et al.* [1998] in the polar cap, poleward of the auroral zone. These scintillations are produced by ionospheric irregularities created in the *F* region density gradients associated with polar cap patches [*Coker et al.*, 2004]. Polar cap patches are 100 km scale regions with *F* region plasma densities roughly 5–10 times larger than the normally low-density *F* region within the polar cap. These patches appear to enter the polar cap on the dayside, drift toward midnight, and exhibit structuring on the leading and trailing edges that is presumed to be created by the gradient drift instability and lead to irregularities [*Buchau et al.*, 1984]. These irregularities typically do not produce diffractive scintillations at GPS L-band frequencies because the ionospheric densities are too small. However, refractive scintillations in the form of the time rate of change of TEC were reported by *Basu et al.* [1998], who observed TEC changing by 2 TECU min^{-1} on the edges of polar cap patches with peak VTEC values of about 10 TECU. *Aarons* [1997] studied similar GPS phase fluctuations from 12 receivers distributed over geomagnetic latitude from 54° to 85° also using the measure of TECU min^{-1}. He concludes that the phase fluctuations are largest in the auroral oval near magnetic midnight. In the polar cap the phase fluctuations were less intense. During periods of magnetic activity the phase fluctuations increase in intensity and move equatorward along with the auroral oval. Aarons was not able to determine the irregularity altitude, suggesting that it may come from either the *E* or *F* region, depending on auroral activity.

[98] Occasional observations of GPS amplitude scintillations in the auroral oval have been reported. For

example, brief GPS amplitude scintillations have been reported recently but their origin is still under investigation (C. Mitchell, private communication, 2006). In addition, *Aarons* [1997] reported on a symposium paper by Bishop and Holland where L2 amplitude scintillations produced $S_4 = 0.4$.

[99] In addition to *F* region polar cap patches, *E* region ionization associated with auroral electron precipitation can potentially cause fluctuating TEC values, yielding refractive scintillations. *Coker et al.* [1995] investigated this possibility using the time rate of change of TEC as a measure of activity. The difficulty in this approach is that both the *F* region and *E* region contribute to TEC. They developed a technique using high pass-filtered time rate of change of TEC to isolate examples that exceeded 2 TECU min^{-1} and validated their approach with HF propagation anomalies, auroral magnetometer disturbances, and satellite measurements of electron precipitation to demonstrate that *E* region ionization was causal. This technique was capable of detecting both broad areas of *E* region ionization as well as the equatorward border of the auroral oval.

[100] Individual auroral arcs producing refractive scintillations or simply rapid changes in TEC was first demonstrated by *Kintner et al.* [2002], who observed two rapid TEC spikes of about 8 TECU lasting about 5 min and 3 min, respectively. Using all-sky camera data, the TEC spikes were shown to be coincident with the passage of auroral arcs at low elevations ($10°-15°$). Further analysis of the *E* region ionization implied by the all-sky camera images demonstrated that for the large slant factor, the TEC changes were consistent with the inferred ionization.

[101] Similar refractive scintillations were observed during an auroral substorm at Poker Flat, Alaska. The observation was during an auroral brightening, signaling the onset of a 250 nT magnetic bay on 6 March 2005. A very bright auroral arc appeared nearly overhead on the path of a GPS satellite signal. Figure 16 shows four images documenting the arc brightening. South is at the top and east is at the right of each image. The red dot is the elevation and azimuth of PRN 23. An arc begins to appear overhead at 0633:35 UT then brightens until becoming very intense at 0637:36. At 0642:06 the arc has lost some its intensity, moved just poleward of the GPS signal path, and a poleward arc has developed. The overhead arc continues to decline in intensity at 0646:35 and the auroral breakup is now clearly visible to the north.

[102] The TEC measured from PRN 23 is shown in Figure 17. There is an increase in TEC of about 5 TECU from 0636 to 0642 corresponding to the period of bright arcs on the GPS signal path. When the brightest arc was present at 0637, the GPS receiver experienced a cycle slip. The cause of the cycle slip is unknown but was most likely caused by a rapid change in the TEC. The possibility of edge diffraction on a step density gradient produced by the bright auroral arc cannot be ruled out but fast signal amplitude data were not available for this measurement. The rapid changes in TEC coincident with the bright auroral arc support the conclusion of *Coker et al.* [1995] that *E* region ionization is the causal factor of fast TEC fluctuations at high latitudes.

7. Future Directions

[103] The investigation of scintillations, understanding their impact on GPS as well as other GNSS receivers, and mitigating the operational and safety concerns will continue to evolve as the implementation of satellite navigation evolves. The preceding has considered GPS as a stand-alone system with signals and codes developed in the 1970s. In the next decade much will change. Already GPS is being aided by differential systems such as the Wide Area Augmentation System (WAAS) and the European Geodetic Navigation Overlay System (EGNOS). The first satellites testing signals for both the modernized GPS L2 civilian code and the European Galileo system were launched in 2005. The Russian satellite navigation system, called GLONASS, is being revitalized with new spacecraft. As GPS is fully modernized and Galileo becomes operational, several new signals and codes will become available that will continue to be vulnerable to scintillations.

[104] Differential systems depend on reference receivers on the ground that calculate ranging errors to their known positions and then distribute these errors to mobile receivers. In distributing these errors, both WAAS and EGNOS use the L1 frequency with a C/A PRN code so that, to a receiver, the RF and tracking are the same as for the GPS satellite signals. Forward error correction is used in transmitting the data, protecting against fades of less than 0.1 s. The vulnerability of the WAAS message to scintillations (fading) has been investigated by *Doherty et al.* [2002] and found to be significant, leading to the requirement that at least two SBAS satellites be visible to aircraft in order to make loss of data less likely. There is evidence that the dual-frequency semicodeless reference receivers are much more vulnerable than L1 single frequency receivers [*Skone*, 2001], as discussed in section 3.4, which will directly affect WAAS and EGNOS. Additionally, differential systems are vulnerable to ionospheric gradients in both space and time. The coarse spacing (approximately 25 reference receivers for WAAS across the United States) and the lengthy message update period (6 min for WAAS) cannot resolve the rapid changes in the midlatitude ionosphere during magnetic storms. Indeed the FAA has noted that "The ionosphere may be thought of as the battleground between WAAS and the Sun" (SatNav News, volume 23, June 2004). Efforts to extend the WAAS design to tropical regions will encounter more frequent and more severe diffractive and refractive ionospheric scintillations than are typically found at midlatitudes. Similar to WAAS, a Local Area Augmentation System (LAAS) is being designed for navigation at individual airports and to enable category III landings (decision height of 30 m or less, runway visual range of 200 m or less). The architecture for LAAS is currently

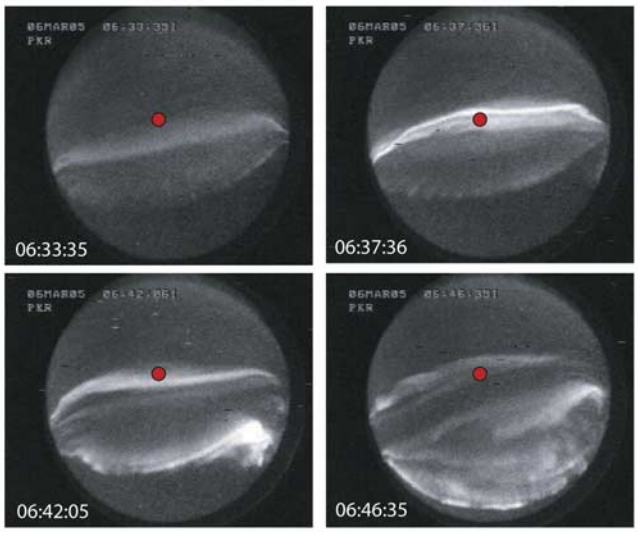

Figure 16. All-sky camera picture of an auroral breakup on 6 March 2005. The red dot is the elevation and azimuth of GPS satellite PRN 27. South is at the top and east is to the right of each image. The camera was located at the Poker Flat Research Range in Alaska.

being designed but it will need to create ranging corrections for a least a few tens of kilometers, which corresponds to known ionospheric gradient scale lengths during magnetic storms, and the reference receivers will also be vulnerable to scintillations as noted above.

[105] Many of the vulnerabilities of differential systems can be mitigated with dual-frequency architectures, which will be the next step in GPS modernization, beginning with the new civilian signal on L2 and later with an L5 signal in a protected band for civil aviation. Dual-frequency systems measure and can remove the refractive effects of the ionosphere where signal propagation is dispersive.

[106] As mentioned in section 3.4, the advent of L2C will provide a significant improvement over current semicodeless receivers in their ability to track dual-frequency signals, particulary when the signals are weak or are experiencing fluctuations in phase and amplitude. Many of the dropouts experienced by semicodeless dual-frequency receivers occur during ionospheric storms and are likely associated with fast phase fluctuations due to high plasma convection velocities [*Skone*, 2001]. In scintillating environments, these receivers do not stand a chance to track the fluctuating GPS signals that clearly fade to levels far below the nominal 35 dB-Hz tracking limit. Civilian dual-frequency receivers using GPS L1 and either L2C or L5 will operate more reliably and robustly during ionospheric storms and in scintillating environments. This improvement translates into improved navigation performance for civilian dual-frequency users. It will also allow for TEC and scintillation measurements at times when, arguably, the physics is most interesting.

[107] Potentially the most significant evolution in satellite navigation will come with the initiation of the European Galileo navigation system early in the next decade. Galileo will provide 30 additional navigation satellites in medium-Earth orbit, transmitting 10 different navigation signals. The signals are classified as open access, safety of life, search and rescue, commercial service, and public-regulated service. The open-access and safety-of-life signals will be unencrypted and civilian accessible, while the search and rescue, commercial service, and public-regulated service signals will be encrypted. The signals' naming conventions, carrier frequencies, and code and data bit modulation schemes are sufficiently complex that the interested reader should consult references such as *Hein et al.* [2002]. The remainder of the discussion on Galileo will focus on open-access signals.

[108] The three open access signals are called E5a, E5b, and L1B. L1B and E5a are transmitted at carrier frequencies that are the same as the GPS L1 (1575.42 MHz) and GPS L5 (1176.45 MHz) frequencies, respectively. These open access signals have been designed to be interoperable with the civilian-accessible GPS signals at L1 and L5. The L1B and E5a signals have the same respective chipping rates as the GPS L1 C/A (1.023 chips/s) and L5 (10.23 chips/s) signals but use different modulation schemes. The primary difference in the Galileo modulation schemes is the use of binary offset carrier (BOC) modulation, which mixes the PRN code with a square-wave subcarrier at a frequency that is an integer multiple of the chipping rate. BOC modulation provides two important characteristics. First, it adjusts the power spectra

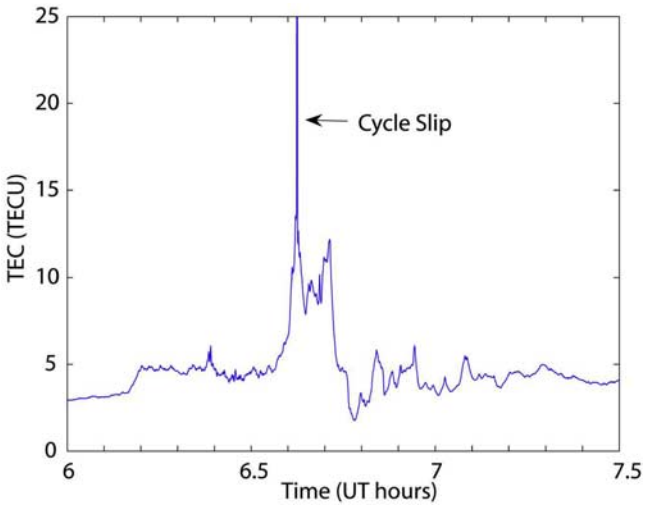

Figure 17. TEC measured from PRN 27 on 6 March 2005 UT. The receiver is located at the Poker Flat Research Range in Alaska. The period of TEC measurements corresponds to that shown in Figure 16.

of the Galileo signals by moving power away from the carrier signal, which decreases interference with GPS signals at the same carrier frequency. Second, the BOC modulation has been shown to provide slightly improved ranging and multipath mitigation with respect to the BPSK modulation used in the GPS signals [*Hein et al.*, 2002].

[109] The interference between GPS and Galileo is a potential concern when tracking scintillating signals because it can raise the threshold for loss of lock. Nevertheless, the interference has been shown to be small, a result of the careful design of Galileo signals, typically less than 0.05 dB for L1 signals and less than 0.5 dB for L5 signals [*Godet et al.*, 2002]. These degradations are small compared to the deep fades that GNSS signals experience during scintillations.

[110] It is likely that future dual-frequency receivers for investigating the ionosphere will skip L2C in favor of L5. This assertion is supported by the presence of only two open Galileo signals centered at the L1 and L5 frequencies. Thus designing a hybrid GPS/Galileo receiver (particularly the RF front end) to use L1 and L5 frequencies is significantly easier because the signals are in the same RF bands.

[111] The main advantage that Galileo will offer ionospheric scientists over the next decade is a doubling of the number of TEC and scintillation measurement data points. This doubling will result in more accurate three-dimensional imaging and TEC maps and an improved understanding of ionospheric physics via assimilative models. Note that the increase in data from Galileo and the increase in the number of scientific-grade GNSS receivers on the ground and in space will likely produce a large computational burden on assimilative models and imaging techniques that already require computer clusters to operate in real time.

8. Conclusions

[112] In less than a decade, GPS and satellite navigation has developed from an esoteric science and engineering topic to a household word. Application of these systems deeper into our technological infrastructure will depend not only on their accuracy but on their reliability and integrity as well. While using GPS to create directions for driving is commonly accepted, no one wants GPS to actually drive the car, or at least, not yet. Within the next few years GPS will be used increasingly in life-critical applications such as civil aviation, applications will require greater accuracy, and uninterrupted service will be necessary. Given this future, one may well ask what the societal effects of scintillations at L-band frequencies will be.

[113] In the near term, i.e., the next 5–7 years through solar maximum and before GPS is fully modernized and Galileo is inaugurated, the largest source of errors will be the ionosphere. These errors will be more severe during solar maximum when the ionosphere is the densest. GPS assets that were installed during solar minimum will be tested for the first time during solar maximum. For life-critical applications, the approach to assuring safety is to reduce operational availability. In those cases in which space weather is not well understood, such as midlatitude scintillations, the approach to reducing operational availability must be conservative. GPS will certainly enable more reliable and precise navigation overall but one should still expect space weather delays in air travel during the next solar maximum. In some cases, especially in the tropics, it will be unwise to rely on GPS alone for navigation.

[114] After 2014 both Galileo and GPS will transmit at L1 and L5, so these frequencies will likely become the standard for removing ionospheric errors in stand-alone receivers. The L5 frequency is 1176.45 MHz compared with the L1 frequency of 1575.42 MHz. The smaller L5 frequency will experience scintillations at longer Fresnel lengths at which, typically, the irregularities are more intense. In addition the lower frequency will experience more phase shift for the same density perturbation, compared to L1. So adding L5 yields a technical solution to coping with refractive scintillations but it will be more sensitive to diffractive scintillations than L1 currently experiences. Currently little, if any, research has investigated the increased vulnerability of the L5 signal. The GPS L2C (1227.5 MHz) signal is nearly the same frequency as the L5 signal and is also more vulnerable to scintillations than L1.

[115] On the other hand, new GPS receiver technology along with new signals will usher in a new era of ionospheric science. The first dividends are already being paid with CORS and other networks, which have revealed midlatitude ionospheric storms [*Coster et al.*, 2005]. In Japan a dense network of more than 1000 TEC receivers produce image-quality maps of TEC that reveal the existence of wave-like structures with peak-to-peak values of up to 30 TECU that propagate across Japan. Imaging of irregularities that cause ionospheric scintillations by using arrays of receivers will become a reality when truly inexpensive TEC receivers become available. This improvement, along with other notable steps in understanding scintillations, from measuring the properties of irregularities that produce them to understanding the instabilities behind their development, will pave the way to better models for irregularity development and, eventually, scintillation prediction.

[116] **Acknowledgments.** This research was supported by ONR grant N00014-04-1-0105. The authors gratefully acknowledge the contributions of colleagues M. Psiaki, T. Humphreys, A. Cerruti, T. Beach, C. N. Mitchell, A. Saito, A. Coster, and I. Kantor.

References

Aarons, J. (1982), Global morphology of ionospheric scintillations, *Proc. IEEE*, *70*, 360–378.

Aarons, J. (1997), Global positioning system phase fluctuations at auroral latitudes, *J. Geophys. Res.*, *102*, 17,219–17,231.

Aarons, J., and S. Basu (1994), Ionospheric amplitude and phase fluctuations at the GPS frequencies, paper presented at ION GPS, Inst. of Navig., Salt Lake City, Utah.

Aarons, J., J. P. Mullen, H. E. Whitney, and E. M. MacKenzie (1980a), The dynamics of equatorial irregularity patch formation, motion, and decay, *J. Geophys. Res.*, *85*, 139–149.

Aarons, J., J. P. Mullen, J. P. Koster, R. F. DaSilva, J. R. Medeiros, R. T. Medeiros, A. Bushby, J. Pantoja, J. Lanat, and M. R. Paulson (1980b), Seasonal and geomagnetic control of equatorial scintillations in two longitudinal sectors, *J. Atmos. Terr. Phys.*, *42*(9–10), 861–866.

Aarons, J., J. A. Klobuchar, H. E. Whitney, J. Austen, A. L. Johnson, and C. L. Rino (1983), Gigahertz scintillations associated with equatorial patches, *Radio Sci.*, *18*, 421–434.

Anderson, D. N., and G. Haerendel (1979), Motion of depleted plasma regions in the equatorial ionosphere, *J. Geophys. Res.*, *84*, 4251–4256.

Basu, S., S. Basu, J. P. Mullen, and A. Bushby (1980), Long-term 1.5 GHz amplitude scintillation measurements at the magnetic equator, *Geophys. Res. Lett.*, *7*, 259–262.

Basu, S., E. MacKenzie, and Su. Basu (1988), Ionospheric constraints on VHF/UHF communication links during solar maximum and minimum periods, *Radio Sci.*, *23*, 363–378.

Basu, S., E. J. Weber, T. W. Bullett, M. J. Keskinen, E. MacKenzie, P. Doherty, R. Sheehan, H. Kuenzler, P. Ning, and J. Bongiolatti (1998), Characteristics of plasma structuring in the cusp/cleft region at Svalbard, *Radio Sci.*, *33*, 1885–1900.

Basu, S., et al. (2001), Ionospheric effects of major magnetic storms during the international space weather period of September and October 1999: GPS observations, VHF/UHF scintillations, and in situ density structures at middle and equatorial latitudes, *J. Geophys. Res.*, *106*, 30,389–30,414.

Basu, Su., et al. (2005), Two components of ionospheric plasma structuring at midlatitudes observed during the large magnetic storm of October 30, 2003, *Geophys. Res. Lett.*, *32*, L12S06, doi:10.1029/2004GL021669.

Beach, T. L. (1998), Global Positioning System studies of equatorial scintillations, Ph.D. thesis, Cornell Univ., Ithaca, N. Y.

Beach, T. L. (2006), Perils of the GPS phase scintillation index (Sigma Phi), *Radio Sci.*, *41*, RS5S31, doi:10.1029/2005RS003356.

Booker, H. G., and H. W. Wells (1938), Scattering of radio waves by the *F*-region of the ionosphere, *Terr. Magn. Atmos. Elect.*, *43*, 249–256.

Booker, H. G., J. A. Ratcliffe, and D. H. Shinn (1950), Diffraction from an irregular screen with applications to ionospheric problems, *Phil. Trans. R. Soc. London, Ser. A*, *856*, 579–609.

Briggs, B. H. (1964), Observations of radio star scintillations and spread-F echoes over a solar cycle, *J. Atmos. Terr. Phys.*, *26*, 1–23.

Briggs, B. H., and I. A. Parkin (1963), On the variation of radio star and satellite scintillation with zenith angle, *J. Atmos. Terr. Phys.*, *25*, 339–365.

Buchau, J., E. J. Weber, D. N. Anderson, H. C. Carlson Jr., J. G. Moore, B. W. Reinisch, and R. C. Livingston (1984), Ionospheric structures in the polar cap: Their origin and relation to 250-MHz scintillation, *Radio Sci.*, *20*, 325–338.

Buckley, R. (1975), Diffraction by a random phase-changing screen: A numerical experiment, *J. Atmos. Terr. Phys.*, *37*, 1431–1446.

Bust, G. S., T. W. Garner, and T. L. Gaussiran II (2004), Ionospheric Data Assimilation Three-Dimensional (IDA3D): A global, multisensor electron density specification algorithm, *J. Geophys. Res.*, *109*, A11312, doi:10.1029/2003JA010234.

Cerruti, A. P., B. M. Ledvina, and P. M. Kintner (2005), Measurements of equatorial scintillations on the WAAS satellite, paper presented at IES 2005, 11th International Ionospheric Effects Symposium, Radio Propag. Serv., Alexandria, Va.

Coker, C., R. Hunsucker, and G. Lott (1995), Detection of auroral activity using GPS satellites, *Geophys. Res. Lett.*, *22*, 3259–3262.

Coker, C., G. S. Bust, R. A. Doe, and T. L. Gaussiran II (2004), High-latitude plasma structure and scintillation, *Radio Sci.*, *39*, RS1S15, doi:10.1029/2002RS002833.

Conker, R. S., M. B. El-Arini, C. J. Hegarty, and T. Hsiao (2003), Modeling the effects of ionospheric scintillation on GPS/satellite-based augmentation system availability, *Radio Sci.*, *38*(1), 1001, doi:10.1029/2000RS002604.

Coster, A., S. Skone, C. Mitchell, G. De Franceschi, L. Alfonso, and V. Romano (2005), Global studies of GPS scintillation, paper presented at National Technical Meeting (NTM 2005), Inst. of Navig., San Diego, Calif.

Dehel, T., F. Lorge, and J. Waburton (2004), Satellite navigation vs. the ionosphere: Where are we, and where are we going?, paper presented at ION GPS 2004, Inst. of Navig., Long Beach, Calif.

de Rezende, L. F. C., E. R. de Paula, I. J. Kantor, and P. M. Kintner (2007), Mapping and survey of plasma bubbles over Brazilian territory, *Navigation*, in press.

Doherty, P. H., T. Dehel, J. A. Klobuchar, S. H. Delay, S. Datta-Barua, E. R. de Paula, and F. S. Rodrigues (2002), Ionospheric effects on low-latitude space-based augmentation systems, paper presented at ION GPS 2002, Inst. of Navig., Portland, Oreg.

Doherty, P. H., T. Walter, D. Bunce, T. Dehel, and T. McHugh (2004), Space weather effects on WAAS: A performance and status report, paper presented at Beacon Satellite Symposium 2004, Int. Cent. for Theor. Phys., Trieste, Italy.

Forte, B. (2005), Optimum detrending of raw GPS data for scintillation measurements at auroral latitudes, *J. Atmos. Sol. Terr. Phys.*, *67*(12), 1100–1109, doi:10.1016/j.jastp.2005.01.011.

Forte, B., and S. M. Radicella (2002), Problems in data treatment for ionospheric scintillation measurements, *Radio Sci.*, *37*(6), 1096, doi:10.1029/2001RS002508.

Foster, J. C., and H. B. Vo (2002), Average characteristics and activity dependence of the subauroral polarization stream, *J. Geophys. Res.*, *107*(A12), 1475, doi:10.1029/2002JA009409.

Foster, J. C., P. J. Erickson, F. D. Lind, and W. Rideout (2004), Millstone Hill coherent-scatter radar observations of electric field variability in the sub-auroral polarization stream, *Geophys. Res. Lett.*, *31*, L21803, doi:10.1029/2004GL021271.

Fremouw, E. J., and J. A. Secan (1984), Modeling and application of scintillation results, *Radio Sci.*, *19*, 687–694.

Fremouw, E. J., R. C. Livingston, and D. Miller (1980), On the statistics of scintillating signals, *J. Atmos. Terr. Phys.*, *42*, 717–731.

Godet, J., J. C. de Mateo, P. Erhard, and O. Nouvel (2002), Assessing the radio frequency compatibility between GPS and Galileo, paper presented at ION GPS 2002, Inst. of Navig., Portland, Oreg.

Hajj, G. A., B. D. Wilson, C. Wang, X. Pi, and I. G. Rosen (2004), Data assimilation of ground GPS total electron content into a physics-based ionospheric model by use of the Kalman filter, *Radio Sci.*, *39*, RS1S05, doi:10.1029/2002RS002859.

Hein, G. W., J. Godet, J.-L. Issler, J.-C. Martin, P. Erhard, R. Lucas-Rodriguez, and T. Pratt (2002), Status of Galileo frequency and signal design, paper presented at ION GPS 2002, Inst. of Navig., Portland, Oreg.

Hewish, A. (1951), The diffraction of radio waves in passing through a phase-changing ionosphere, *Proc. R. Soc. London, Ser. A*, *209*, 81–96.

Hey, J. S., S. J. Parsons, and J. W. Phillips (1946), Fluctuations in cosmic radiation at radio-frequencies, *Nature*, *158*, 234.

Humphreys, T. E., M. L. Psiaki, and P. M. Kintner Jr., and B. M. Ledvina (2005), GPS carrier tracking loop performance in the presence of ionospheric scintillations, paper presented at ION GNSS 2005, Inst. of Navig., Long Beach, Calif.

Kelley, M. C. (1985), Equatorial spread *F*: Recent results and outstanding problems, *J. Atmos. Terr. Phys.*, *47*, 745–752.

Kelley, M. C., F. Garcia, J. Makela, T. Fan, E. Mak, C. Sia, and D. Alcocer (2000), Highly structured tropical airglow and TEC signatures during strong geomagnetic activity, *Geophys. Res. Lett.*, *27*(4), 465–468.

Kelley, M. C., J. J. Makela, B. M. Ledvina, and P. M. Kintner (2002), Observations of equatorial spread *F* from Haleakala, Hawaii, *Geophys. Res. Lett.*, *29*(20), 2003, doi:10.1029/2002GL015509.

Kent, G. S. (1959), High frequency fading observed on the 40 Mc/s wave radiated from artificial satellite 1957a, *J. Atmos. Terr. Phys.*, *16*, 10–20.

Keskinen, M. J., S. Basu, and S. Basu (2004), Midlatitude sub-auroral ionospheric small scale structure during a magnetic storm, *Geophys. Res. Lett.*, *31*, L09811, doi:10.1029/2003GL019368.

Kil, H., P. M. Kintner, E. R. de Paula, and I. J. Kantor (2000), Global Positioning System measurements of the ionospheric zonal apparent velocity at Cachoeira Paulista in Brazil, *J. Geophys. Res.*, *105*, 5238–5317.

Kintner, P. M., H. Kil, and E. de Paula (2001), Fading timescales associated with GPS signals and potential consequences, *Radio Sci.*, *36*, 731–743.

Kintner, P. M., H. Kil, C. Deehr, and P. Schuck (2002), Simultaneous total electron content and all-sky camera measurements of an auroral arc, *J. Geophys. Res.*, *107*(A7), 1127, doi:10.1029/2001JA000110.

Kintner, P. M., B. M. Ledvina, E. R. de Paula, and I. J. Kantor (2004), Size, shape, orientation, speed, and duration of GPS equatorial anomaly scintillations, *Radio Sci.*, *39*, RS2012, doi:10.1029/2003RS002878.

Klobuchar, J. A., P. H. Doherty, and M. B. El-Arini (1995), Potential ionospheric limitations to GPS wide-area augmentation system (WAAS), *Navigation*, *42*, 353–370.

Ledvina, B. M., and J. J. Makela (2005), First observations of SBAS/WAAS scintillations: Using collocated scintillation measurements and all-sky images to study equatorial plasma bubbles, *Geophys. Res. Lett.*, *32*, L14101, doi:10.1029/2004GL021954.

Ledvina, B. M., J. J. Makela, and P. M. Kintner (2002), First observations of intense GPS L1 amplitude scintillations at midlatitude, *Geophys. Res. Lett.*, *29*(14), 1659, doi:10.1029/2002GL014770.

Ledvina, B. M., P. M. Kintner, and J. J. Makela (2004), Temporal properties of intense GPS L1 amplitude scintillations at midlatitudes, *Radio Sci.*, *39*, RS1S18, doi:10.1029/2002RS002832.

Lovelace, R. V. E. (1970), Theory and analysis of interplanetary scintillations, Ph.D. thesis, Cornell Univ., Ithaca, N. Y.

Makela, J. J., M. C. Kelley, J. J. Sojka, X. Pi, and A. J. Mannucci (2001), GPS normalization and preliminary modeling results of total electron content during a midlatitude space weather event, *Radio Sci.*, *36*, 351–362.

Mishin, E. V., W. J. Burke, C. Y. Huang, and F. J. Rich (2003a), Electromagnetic wave structures within subauroral polarization streams, *J. Geophys. Res.*, *108*(A8), 1309, doi:10.1029/2002JA009793.

Mishin, E. V., W. J. Burke, S. Basu, S. Basu, P. M. Kintner, and B. Ledvina (2003b), Stormtime ionospheric irregularities in SPAS-related troughs: Causes of GPS scintillations at mid-latitudes, *Eos Trans. AGU*, *84*(46), Fall Meet. Suppl., Abstract SH52A-07.

Morrissey, T. N., K. W. Sahlberg, A. J. Van Dierendonck and M. J. Nicholson (2002), GPS receiver performance characterisation under realistic ionospheric scintillation environments II, paper presented at Ionospheric Effects Symposium (IES 2002), Radio Propag. Serv., Alexandria, Va.

Pidwerbetsky, A., and R. V. E. Lovelace (1989), Chaotic wave propagation in a random medium, *Phys. Lett. A*, *140*, 411–415.

Proakis, J. G. (2001), *Digital Communications*, 4th ed., p. 346, McGraw-Hill, New York.

Psiaki, M. L., T. E. Humphreys, S. Mohiuddin, S. P. Powell, A. P. Cerruti, and P. M. Kintner Jr. (2006), Searching for Galileo: Reception and analysis of signals from GIOVE-A, *GPS World*, *17*(6), 66–72.

Rastogi, R. G., and H. W. Kroehl (1978), Interplanetary magnetic field and equatorial ionosphere, *Ind. J. Radio Space Phys.*, *7*(2), 84–89.

Rino, C. L. (1979a), A power law phase screen model for ionospheric scintillation: 1. Weak scatter, *Radio Sci.*, *14*, 1135–1145.

Rino, C. L. (1979b), A power law phase screen model for ionospheric scintillation: 2. Strong scatter, *Radio Sci.*, *14*, 1147–1155.

Rino, C. L., and E. J. Fremouw (1977), The angle dependence of singly scattered wavefields, *J. Atmos. Terr. Phys.*, *39*, 859–868.

Rino, C. L., and J. Owen (1984), Numerical simulations of intensity scintillation using the power law phase screen model, *Radio Sci.*, *19*, 891–908.

Rodrigues, F. S. (2003), Estudo das irregularidades ionoféricas equatoriais utilizando sinais GPS, Master dissertation, Inst. Nac. de Pesqui. Espaciais, São José dos Campos, Brazil.

Saito, A., S. Fukao, and S. Miyazaki (1998), High resolution mapping of TEC perturbations with the GSI GPS network over Japan, *Geophys. Res. Lett.*, *25*, 3079–3082.

Schunk, P. I. M. (1995), A global ionospheric parameterization based on first principle models, *Radio Sci.*, *30*, 1499–1510.

Skone, S. H. (2001), The impact of magnetic storms on GPS receiver performance, *J. Geodesy*, *75*(9--10), 457--468, doi:10.1007/s001900100198.

Sojka, J. J., D. Rice, V. Eccles, T. Berkey, P. Kintner, and W. Denig (2004), Understanding midlatitude space weather: Storm impacts observed at Bear Lake Observatory on 31 March 2001, *Space Weather*, *2*, S10006, doi:10.1029/2004SW000086.

Spilker, J. J., Jr. (1996), GPS signal structure and theoretical performance, in *Global Positioning Systems: Theory and Applications*, vol. *1*, Am. Inst. of Aeronaut. and Astronaut., Washington, D. C.

Tatarskii, V. I. (1971), *The Effects of the Turbulent Atmosphere on Wave Propagation*, Nat. Tech. Inform. Serv., Springfield, Va.

Tsunoda, R. T. (1985), Control of the seasonal and longitudinal occurrence of equatorial scintillations by the longitudinal gradient in integrated E region Pedersen conductivity, *J. Geophys. Res.*, *90*, 447–456.

Van Dierendonck, A. J. (1996), GPS receivers, in *Global Positioning System: Theory and Applications*, vol. *I*, edited by B. Parkinson and J. Spilker Jr., Am. Inst. of Aeronaut. and Astronaut., Washington, D. C.

Whitney, H. E., and S. Basu (1997), The effect of ionospheric scintillation VHF/UHF satellite communication, *Radio Sci.*, *12*, 123–133.

Yeh, C., and C. H. Liu (1982), Radio wave scintillations in the ionosphere, *Proc. IEEE*, *70*, 324–360.

E. R. de Paula, Instituto Nacional de Pesquisas Espaciais, DAE, Av. dos Astronautas 1758, 12.227-010, São Josédos Campos, São Paulo, Brazil. (eurico@dae.inpe.br)

P. M. Kintner, School of Electrical and Computer Engineering, Cornell University, 302 Rhodes Hall, Ithaca, NY 14853, USA. (pmk1@cornell.edu)

B. M. Ledvina, Applied Research Laboratories, University of Texas at Austin, P.O. Box 8029, Austin, TX 78713, USA. (bml22@cornell.edu)